Accepted for publication in **Journal of Materials Engineering and Performance on 3.12.2021**

Experimental investigation on microwave sintered composite tool for electro-discharge machining of Titanium alloy

Anshuman Kumar Sahu [1*], Siba Sankar Mahapatra[1], Neeraj Kumar Bhoi[2], Harpreet Singh[2], Marco Leite[3] and Saurav Goel[4,5]

[1]Department of Mechanical Engineering, National Institute of Technology Rourkela, India

[2]Department of Mechanical Engineering, PDPM IIITDM Jabalpur, India

[3]IDMEC, Instituto Superior Técnico, Universidade de Lisboa, Lisboa, Portugal

[4]School of Engineering, London South Bank University, 103 Borough Road, London SE1 0AA, UK

[5]University of Petroleum and Energy Studies, Dehradun, 248007, India

[*]E-mail: anshuman.sahu123@gmail.com

Abstract: The present study was aimed at investigating the machinability characteristics of titanium alloy (Ti6Al4V) by electro-discharge machining (EDM) process. The machining was performed using composite tools made of Cu-W-B_4C having different compositions manufactured with the help of hybrid microwave sintering (MWS) process. For this experimental investigation, machining performances in terms of material removal rate, tool wear rate and surface characteristics of the machined surfaces were measured as outcomes. The surface characteristics like surface cracks and white layer formation were evaluated with the help of micrographs of the machined surfaces using scanning electron microscope (SEM). Phase identification of the machined surface was carried out with the help of X-ray diffraction (XRD) analysis to identify the effect of sintered tools on the machined surface. The energy dispersive X-ray spectroscopy (EDS) result of the machined surfaces revealed transfer of tool materials (copper and tungsten) onto the machined surface. The removed tool materials deposited on the machined surfaces forms white layer which was found responsible for increasing the micro-hardness of the machined surface. The EDS results of the machined zone were seen in good agreement with the phases identified with XRD analysis with formation of metal carbides such as titanium carbide and vanadium carbide. The study will serve as a testbed in developing a strong link between the MWS composite tool and machining behaviour during EDM of titanium alloys.

Keywords: electro-discharge machining; microwave sintering; composite tool; titanium alloy; surface morphology;

1. Introduction

The quest for better machining performance and the advent class of cutting tool has been key drivers in the manufacturing process industry. The rapid tool wear and deterioration of the cutting edge determine the overall productivity and reliability of the developed strategy. Electro-discharge machining process (EDM) is considered one of the most promising and largely employed non-contact machining processes. EDM process includes machining of very hard materials like forge and die steel, super alloys, hybrid metals and ceramic composites with acute precision which cannot be acquired through the traditional manufacturing processes. The trade-off between sustainable tooling and machining parameters determines the overall quality and service life of manufactured components. The production of sustainable machining tool with the assistance of advanced powder metallurgy has always been a mission for the research community (Ref 1-6). The innovative and novel powder metallurgy and sintering technology with assistance of microwave and spark energy have shown a remarkable tool material suitable for all types of machining. The deteriorated surface characteristics during poor tooling are the main culprit for the shorter service life and product quality. Also, the hazardous emission and scrap during processing limit the machine tool capabilities to a large extent. However, hard coating and conductive medium in the EDM tool material provide the uniform machining quality for a longer period. The processing of tool material plays a vital role in determining the quality of the components.

In the stated context, numerous researchers have tried the combination of different tooling for machining using EDM for a large range of materials (Ref 1, 3-5). Reference can be made to the report given by Khanra et al. (Ref 6) on the performance of the ZrB_2-Cu composite utilized as a tool material for mild steel. They observed that the composite phase of the electrode shows better resistance and material removal rate (MRR) compared to the pure copper (Cu) tool. In the same context, the report was given by Balasubramanian et al. (Ref 7) suggested that the sintered copper electrode performs better compared to the brass and bronze electrodes for machining of EN8 work material. Similarly, the conventional powder metallurgy route was adopted for preparing Cu-20wt.% B_4C electrode for machining SAE 1040 steel material was reported by Cogun et al. (Ref 8). On a comparative assessment given by the research group, it was found that the composite electrode leads to the lowest MRR with a higher electrode wear rate (EWR). The presence of hard inter-metallic compounds on the machined surface in the composite phase exhibits better abrasive resistance. This fact can be correlated to the formation of a recast layer on the machined surface. Gill and Kumar (Ref 9) performed machining of hot die steel (H11) by Cu-Mn powder metallurgy tool. The findings with optimum process parameters show no visible cracks and surface fracture on the machined zone. It was observed that the peak current contributes most of all the process parameters for the machining of H11 steel. It was observed that the formation of inter-metallic compounds such as ferrous carbide

and manganese carbide are the main factors leading to the improvement of surface and wear resistance of the material. The selective surface alerting of the aluminium material using powder metallurgical tool is widely in acceptance for better wear and surface resistant case. The EDM can selectively alter the exposed surface with the exposure to the work material with different coated tools. In this context, the parametric appraisal was assessed with copper tungsten tool material with Taguchi experimental design. The increased surface hardness of the modified surface with composite tooling material was seen to have better wear resistance (Ref 10). Looking at the advantages of the composite tooling for better machining performance, Cu-W electrodes were fabricated by Singh et al. (Ref 11) through conventionally sintering for machining of Al6061-SiC composites. They observed that the recast layer thickness of the machined surface is directly in relation to the supplied discharged energy. It was observed that 30.92% increment in the recast layer thickness with input process settings from the middle stage to a higher stage. It was found that the peak current and pulse on time have a significant influence on the MRR, EWR and roughness value of the machined zone. On a comparable note, Goyal et al. (Ref 12) describe the optimum process conditions for machining of the EN31 die steel with the two different compositions of Cu-Mn tool material. The composite tooling with Cu:Mn (70:30) showed higher surface hardness compared to the Cu-Mn (80:20) and pure copper tool material. The peak current and higher pulse on time were seen as the main influencing factor for improvement in the material hardness of the work material. Looking at the potentials of the composite tool, Cu-CNF electrode was applied by Liew et al. (Ref 13) for machining of resin bonded silicon carbide material (RB-SiC). Looking at the fabricated percentage of the Cu-CNF tool, it was observed that the Cu-1.0 wt.% CNF tool achieved the higher MRR compared to that of the pure Cu electrode. Similar attempts were made by Kumar et al. (Ref 14) for machining of Monel 400 alloy material with Cu-TiB_2 electrode material. The Cu-TiB_2 composite material was prepared with the help of conventional powder metallurgy technique utilizing *V* blender of powder mixing and argon environment sintering (1085 ^{0}C). Five different levels of input process conditions were utilized for the machining behaviour study of the Monel-400 alloy. The optimized process conditions were obtained with multi response surface methodology with desirability approach. It was concluded that the pulse on current was found to be the most influencing parameter for the MRR and EWR. Similarly, composite tools developed by powder metallurgy techniques were also used to form a rigid and wear resistance coated layer on the work piece surface by the EDM process (Ref 1-4, 15-24).

On a comprehensive assessment of the literature, it was observed that no efforts have been made for the development of a hard powder metallurgy tool with the assistance of novel hybrid microwave sintering (MWS) approach. The use of microwave energy is utilized for sintering, cladding, joining and food processing due to their unique heating capabilities. In the present case, microwave sintering is used for the generation of the tool material. The efficacy of the microwave sintering approach for

material development has been reported by numerous researchers. Microwave sintering approach reduces the overall processing time with intense volumetric and selective heating in the bulk metallic material with zero residual and scrap to the environment. MWS implies volumetric and selective heating, rapid and effective diffusion of the reinforcing particles with the matrix elements, shorter processing time and energy saving approach (Ref 25-27). In this paper, a cost effective MWS was utilized for the fabrication of the electrode material for performing the EDM. The present case describes the fabrication of three different composite tools $Cu_{1-x-y}W_xB_4C_y$ (x & y=5, 10 and 15 wt.%) by means of blend press and MWS approach. Till now, the applications of powder metallurgy electrodes during machining of super hard material like titanium and its alloys are rare occurrences in the literature. Therefore, in this work, the machining performance of the MWS electrodes are studied for titanium alloy (Ti6Al4V) and EDM-30 oil as a dielectric medium. Later, the MRR, EWR and microstructure analysis of the machined surfaces were done for the machining of Titanium alloy work material. The comparative assessment was made for the electrode performance in the terms of the outcome of the EDM machining performance.

2. Materials and method

2.1 Preparation of electrode by microwave sintering

In the current study, the tool electrode was manufactured with the help of powder metallurgy and a microwave sintering approach. The initial raw material with a particle size of approximately 44 microns was utilized for the tool manufacturing. For the preparation of the composite tool, copper (Cu), tungsten (W) and boron carbide powders (B_4C) were utilized. Prior to compaction and sintering, the raw powder was mixed homogenously with the use of a planetary ball mill for 8 hours. The mixing of the raw powder was done by varying the percentage of W and B_4C in the Cu. Here, three different weight percentages of W and Cu (i.e. 5, 10 and 15) were used for the composite tool manufacturing. The compaction process of the mixed powder was performed using an automatic uniaxial compaction machine (make: Nano Tec, India) at an applied pressure of 500 MPa with a punch and die system having 10 mm diameter. The compacted billets were subjected to sintering using an innovative bidirectional microwave heating mode. The billets were heated for 15 minutes to 900 ^{0}C using a 900 W, 2.45 GHz domestic microwave oven (make: LG Charcoal oven) with no holding time. The calibration of the temperature was done with the help of radiation pyrometer setting in the oven (Ref 25, 26). During, sintering, silicon plate (SiC) was used as a susceptor material. SiC absorbs the microwave radiation quickly and provides external heating to the billet. The heating process done in the present experiment was termed as a hybrid heating process as it involves the heating of the material from microwave environment and heating the material externally by susceptor medium. For the prevention of the internal wall of the microwave oven and for preventing heat loss to the surroundings, ceramic glass wool (i.e. transparent to microwave radiation) was covered (Ref 25, 26,

28). The sintered billets with a diameter of 10 mm with varying lengths from 8 to 10 mm were obtained. These sintered billets were connected to a copper tool holder with silver conductive glue and were used as the electrode material during the EDM process.

2.2 EDM and collection of performance measures

To study the EDM process with Cu-W-B_4C composite electrodes developed by the MWS process in comparison with solid copper for machining of titanium alloy, a sound experimental procedure was laid out. The EDM machine used was an Electra EMS 5535 (Make: Electronica, India). Regular grade EDM-30 oil was used as a dielectric medium in all the experiments. The input parameters chosen in this work to vary were peak current, pulse-on-time and duty cycle while keeping other parameters unchanged. During machining, the straight polarity of the input conditions was maintained throughout the experiments. A period of 10 minutes was selected for the machining at each experimental setting for different electrodes. The experimental setup is shown in Fig. 1. The different levels of machining conditions are given in Table 1. In the present case, Taguchi's L_{16} experimental design was considered to conduct the experimentations with four factors at four different levels. These details are shown in Table 2. The MRR and TWR were calculated by Eq. (1) and (2) as:

$$\mathrm{MRR} = \frac{1000 \times (W_i - W_f)}{\rho_w \times T} \quad (1)$$

$$\mathrm{TWR} = \frac{1000 \times (W_{ti} - W_{tf})}{\rho_t \times T} \quad (2)$$

W_i= initial sample weight before EDM in g

W_f= final sample weight after EDM in g

T= machining time in min

ρ_w = sample density = 4.42 g/cm^3

W_{ti}=before EDM tool weight in g

W_{tf}=after EDM tool weight in g

ρ_t = density of tool g/cm^3

Archimedes' principle was utilized for the measurements of tool density. The densities of the composite tools were measured by the weight displacement method using a density measurement apparatus equipped with an electronic weight balance machine (CONTECH CA-503, least count=0.001 g). The densities of the tools was found as ρ_{t1} = 8.96 g/cm^3, ρ_{t2} =5.06 g/cm^3, ρ_{t3} =4.94 g/cm^3 and ρ_{t4} =4.64 g/cm^3.

Table 1. Experimental input parameters with their levels

Parameters	Level 1	Level 2	Level 3	Level 4
A: Tool type	Cu (1)	$Cu_{90}W_5(B_4C)_5$ (2)	$Cu_{80}W_{10}(B_4C)_{10}$ (3)	$Cu_{70}W_{15}(B_4C)_{15}$ (4)
B: Peak current (A)	4	6	8	10
C: Pulse-on-time (µs)	50	100	150	200
D: Duty cycle (%)	40	50	60	70

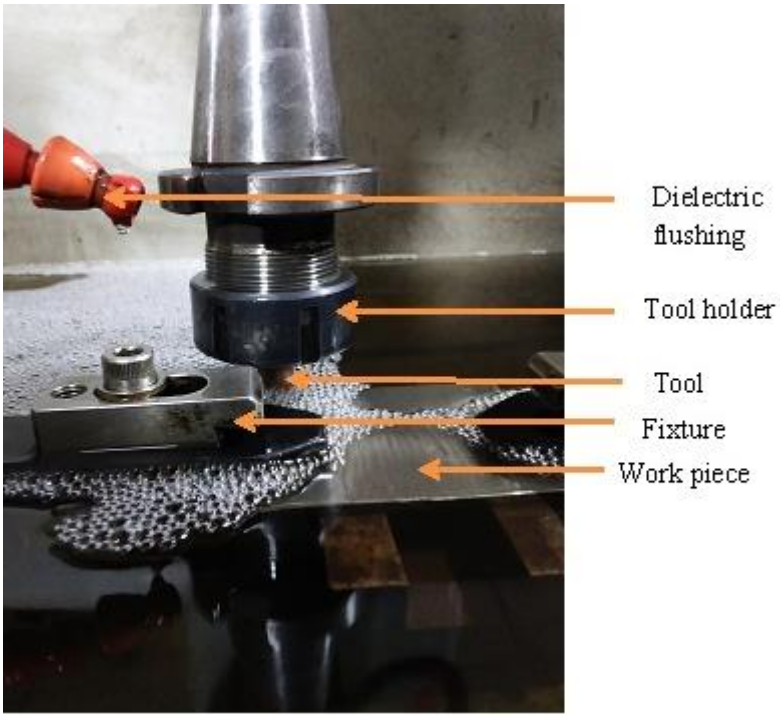

Fig. 1. A photographic view of the machining chamber of EDM experimental setup

The surface roughness measurement was done using a surface tester (model: Surftest SJ 210, Mitutoyo, Japan). The surface crack density (SCD) was measured by taking SEM images of the machined zone by utilizing a scanning electron microscope (SEM) (model: JSM-6480LV, JEOL, Japan). The ratio between the total lengths of the micro-cracks on the machined zone to the area of the SEM image was considered as SCD. On a similar note, the white layer thickness (WLT) was measured by cross-sectional view of the microstructure image showing the deposited layer over the machined zone by using an SEM. WLT was calculated as the ratio of the area of the white layer

present in the micro-graph to the length of the micro-graph. For the measurement of microhardness (MH) of WLT, a Vickers micro-hardness tester (model: LM-248AT, LECO, USA) was utilized. The procedure of measurement of SCD, WLT and MH can also be found in the literature (Ref 29, 30). The surface composition of the machined zone was determined using SEM machine equipped with energy dispersion X-ray spectroscopy (EDX; INCA vx-act, Oxford Instruments, UK) and matching phases were analysed by X-ray diffraction (XRD) (model; D8 advanced, Bruker, Germany). Standard crystallographic data sets were utilized for the identification of the phases formed in the machined zone.

3. Results and discussion

The observed values of performance measures for each experimental setting according to Taguchi's L_{16} design of experiments are shown in Table 2. The effect of machining parameter on the machining outcomes are discussed in the next section.

Table 2. Experimental design and output measures

S. No.	**A (tool)**	**B (A)**	**C (µs)**	**D (%)**	**MRR (mm^3/min)**	**TWR (mm^3/min)**	**Ra (µm)**	**SCD (µm/$µm^2$)**	**WLT (µm)**	**MH**
1	1	4	50	40	0.4525	0.2232	4.30	0.017684	14.318	584.97
2	1	6	100	50	0.6561	0.2675	4.63	0.018596	33.067	632.87
3	1	8	150	60	1.0498	0.4911	5.10	0.020421	33.441	754.53
4	1	10	200	70	1.7195	0.5156	6.40	0.023088	41.796	785.00
5	2	4	100	60	0.6109	1.4384	5.70	0.006316	10.860	662.30
6	2	6	50	70	0.8597	1.6607	6.37	0.008491	8.436	705.70
7	2	8	200	40	0.1627	0.5931	7.83	0.013123	17.717	879.50
8	2	10	150	50	0.1392	1.9273	7.40	0.011860	25.896	860.13
9	3	4	150	70	1.0407	2.0988	9.67	0.004105	19.718	906.40
10	3	6	200	60	0.4525	3.3705	9.50	0.006105	23.894	1173.63

11	3	8	50	50	0.0904	2.7328	8.43	0.005404	24.648	929.13
12	3	10	100	40	0.0396	3.2139	9.20	0.007509	20.452	967.73
13	4	4	200	50	-0.1357	3.3271	12.67	0.004842	83.717	1119.17
14	4	6	150	40	-1.3575	3.7726	12.20	0.005965	113.597	1030.00
15	4	8	100	70	-1.0558	7.4457	14.50	0.005754	119.886	1200.63
16	4	10	50	60	-1.2750	6.2876	14.17	0.005930	116.329	1233.20

3.1. Effect of input parameters on MRR

The influence of the machining parameters as well as tools on the MRR is shown in Fig. 2. Similarly, the variation in MRR as a function of various parameters is shown in Supplementary Fig. 1. The box plot indicates the variation in MRR with the change of tool type. It is to be noted that a solid copper tool allowed achieving the highest MRR. However, a decreasing trend of MRR was observed with an increase in the weight percentage of W and B_4C in the MWS tools. On a similar note, the increasing weight percentage of W and B_4C in the MWS tool increases void percentage rapidly. This phenomenon causes a reduction in the electrical conductivity of the material, eventually reducing the spark energy generated during the machining process leading to a reduced MRR. Generally, an increase in peak current causes MRR to increase due to an increase in spark energy. However, in this work, it was observed that an increase in peak current causes the tool wear to increase. The removed tool materials get deposited on the machined surface. Therefore, a decrease in MRR was observed due to an increase in peak current. The box plot in Supplementary Fig. 1 shows a large variation in MRR with tool type $Cu_{70}W_{15}(B_4C)_{15}$. The higher void content in the tool material leads to an increase in the TWR and deposition of the tool material on the work surface for the MWS tool material with a higher percentage of W and B_4C reinforcement.

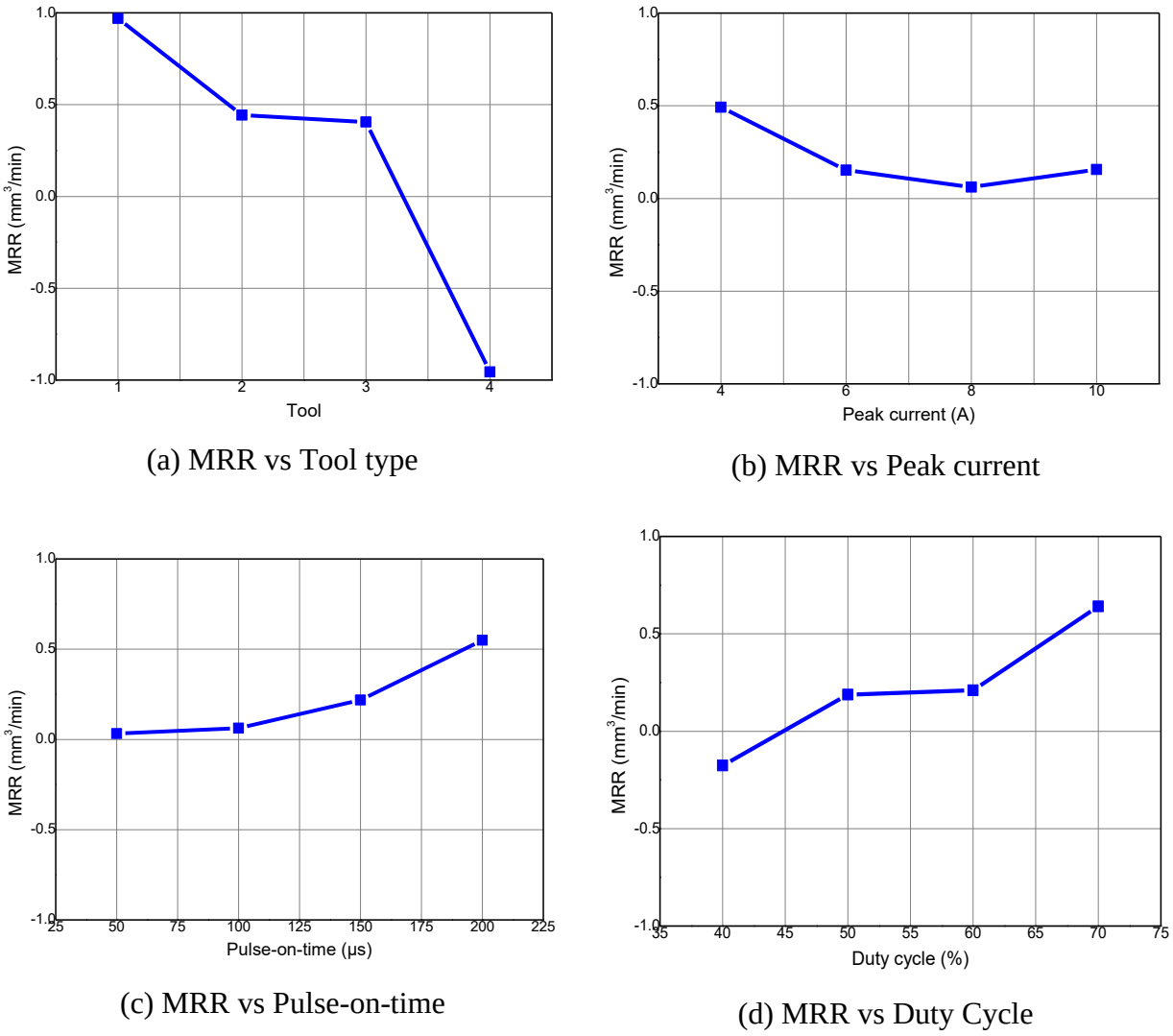

(a) MRR vs Tool type

(b) MRR vs Peak current

(c) MRR vs Pulse-on-time

(d) MRR vs Duty Cycle

Fig. 2. Effect of input parameters on MRR

3.2. Effect of input parameters on TWR

The influence of the machining parameters on TWR is shown in Fig. 3 and the corresponding box-plot for TWR is shown in Supplementary Fig. 2 to show the variation of TWR at different parametric conditions. The minimum TWR was observed for the solid copper tool with higher MRR. However, an increase in W and B_4C percentage on the tool material showed a negative and detrimental effect on the TWR for the composite tool. This may be related to insufficient bonding between the reinforcement and matrix material exhibiting a higher void percentage in the tool. With the increase in peak current and duty cycle, TWR increases due to an increase in spark energy with higher tool wear. However, an increase in pulse-on-time beyond 100 µs decreases the TWR. This may be due to the deposition of carbon element on the tool surface that prevents tool wear. On a similar exploration for machining of Monel alloy, Cu-TiB_2 composite tool showed better MRR with minimal tool wear (Ref 14). The presence of the hard carbide phase on the tool material improves the material erosion and binds the matrix element to a large extent which eventually leads to less tool

wear (Ref 14). The box plot in Supplementary Fig. 2 confirms a small variation in TWR with the use of the solid copper tool. However, a large variation in TWR occurs with the use of tool type of $Cu_{70}W_{15}(B_4C)_{15}$.

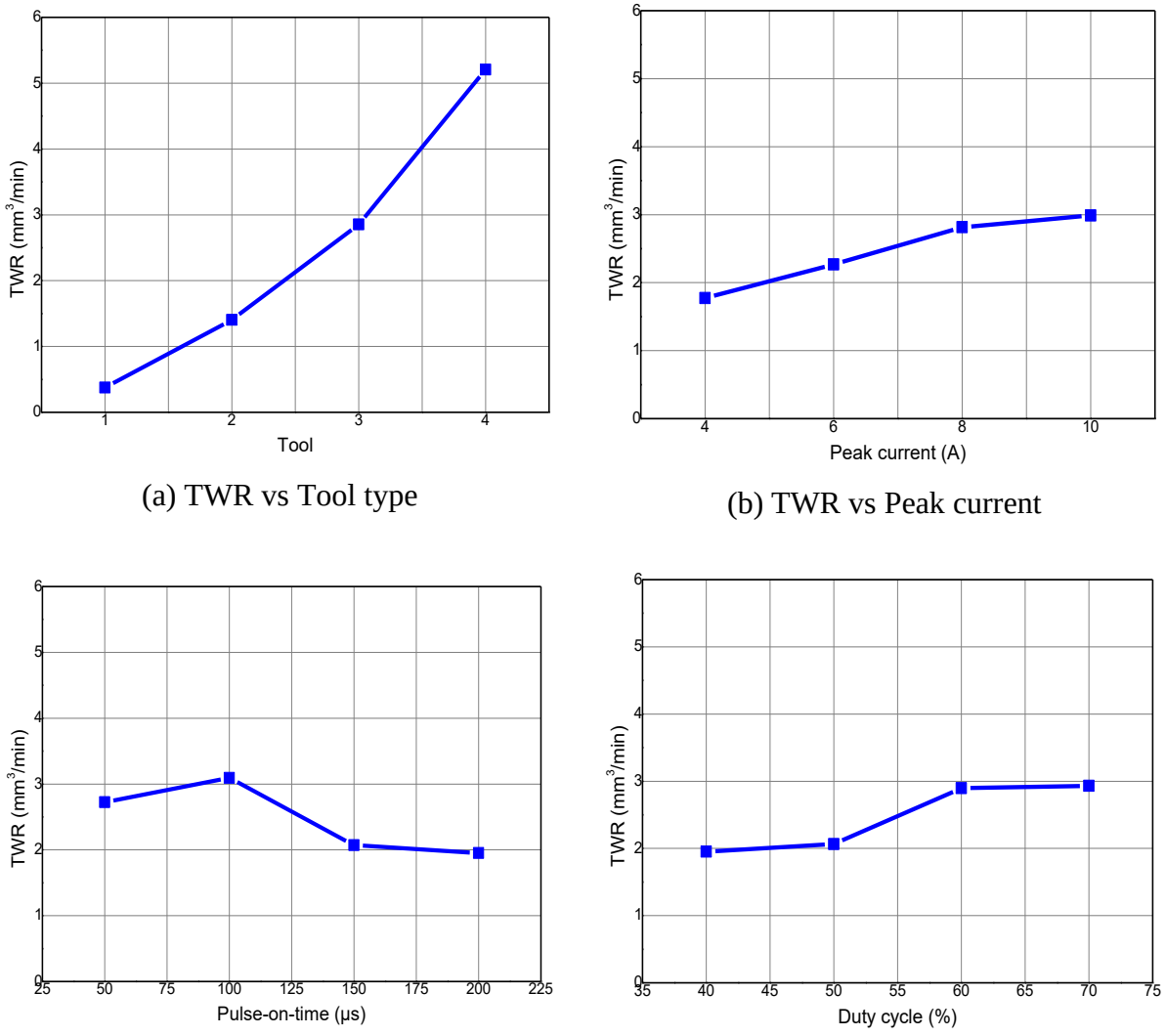

(a) TWR vs Tool type

(b) TWR vs Peak current

(c) TWR vs Pulse-on-time

(d) TWR vs Duty cycle

Fig. 3. Effect of input process parameters on TWR

3.3. Effect of input parameters on Ra

The effect of the input conditions on the surface roughness (R_a) is represented in Fig. 4. Similarly, the box-plot for Ra is shown in Supplementary Fig. 3 to show the variation in the Ra at different parametric conditions. The copper tool showed minimum Ra while the highest Ra was noted for use of the composite tool material. The non-uniform deposition of the reinforcement phase on the cutting zone in the case of the composite tool leads to a rougher surface compared to a monolithic electrode phase. In this context, an increase in peak current and pulse-on-time causes an increase in spark energy which imparts higher roughness owing to the generation of a larger crater area in the cutting zone (Ref 13). With the increase of peak current, the spark energy increases which in turn,

produces a larger crater size during the machining process. From Supplementary Fig. 3, it was observed that the larger variation in R_a was observed with the use of $Cu_{70}W_{15}(B_4C)_{15}$ tool.

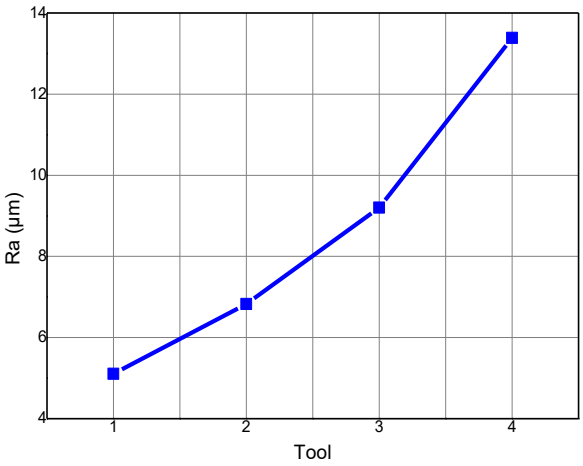

(a) R_a vs Tool type

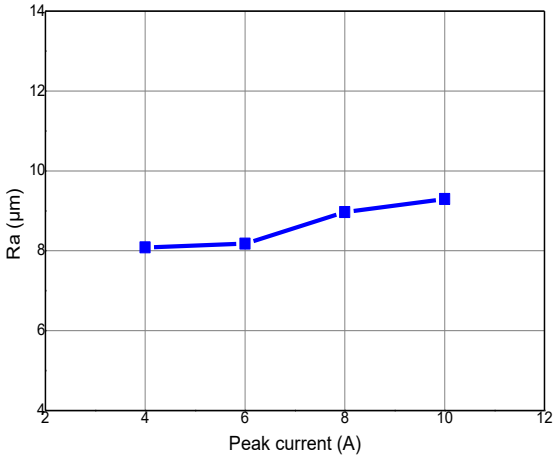

(b) R_a vs Peak Current

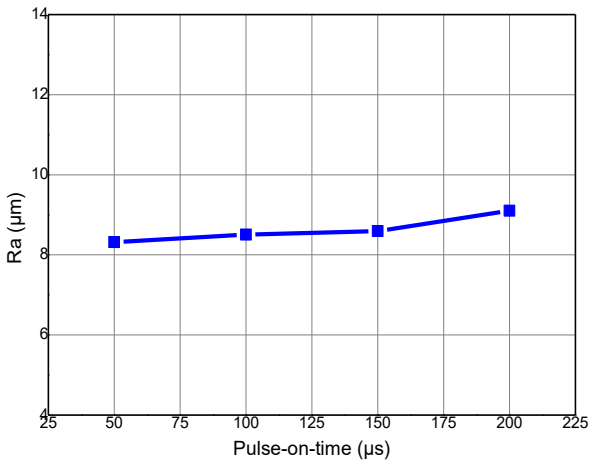

(c) R_a vs Pulse-on-time

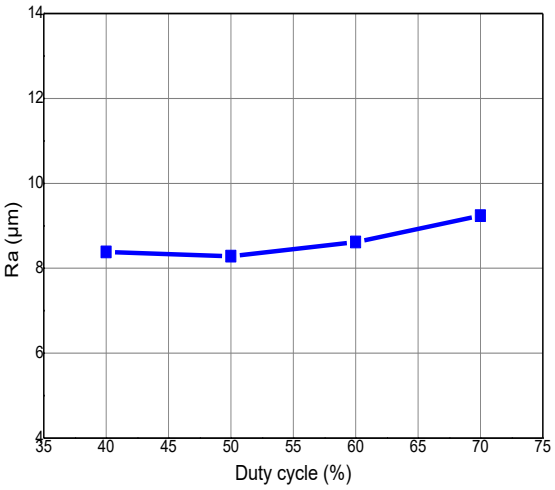

(d) R_a vs Duty cycle

Fig. 4. Effect of input process parameters on R_a

3.4. Effect of input parameters on SCD

Surface cracks are formed on the machined surfaces when the residual strength generated during the sparking process exceeds the ultimate strength. Due to the generation of these micro-cracks, the life of the machined components reduces drastically which affects the overall service life of the component. The effect of machining parameters on SCD is shown in Fig. 5 and the box-plot for SCD is shown in Supplementary Fig. 4 to show the variation in the SCD at different parametric conditions. The solid copper tool shows the highest SCD with decreasing trends with a higher weight percentage of the *W* and B_4C in MWS tools. The residual stress generated on the machined surface becomes less with the presence of *W* and B_4C phases. Therefore, SCD decreases with an increase in the reinforcement percentage of *W* and B_4C in MWS tools as shown in Fig. 6. The increasing trend

of the SCD was noticeable with a higher peak current and pulse on time. However, after a certain point, the SCD tends to reduce with an increase in the duty cycle. The box plot shown in Supplementary Fig. 4 confirms that variation in SCD is reasonably higher with the use of the solid copper tool.

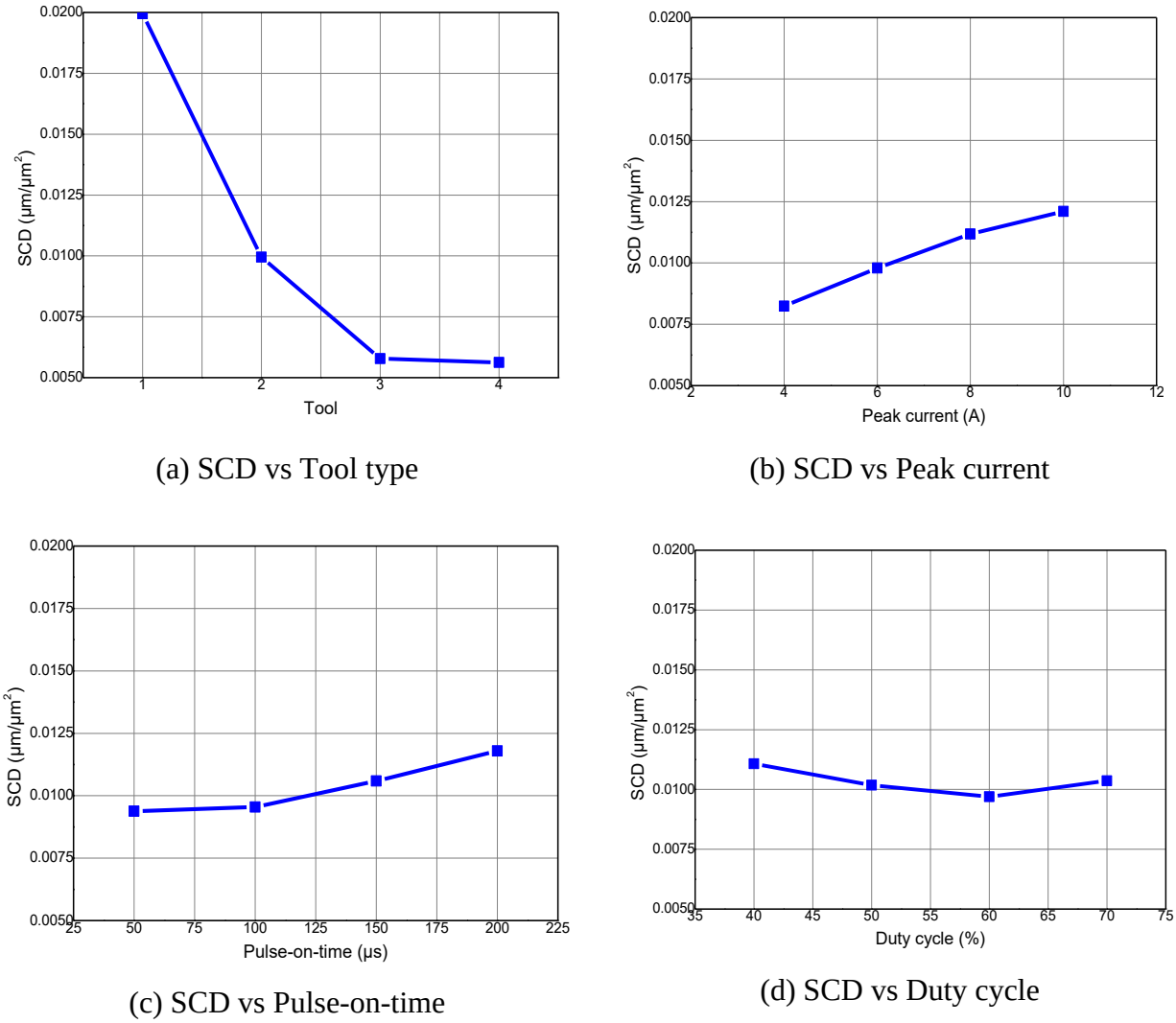

(a) SCD vs Tool type

(b) SCD vs Peak current

(c) SCD vs Pulse-on-time

(d) SCD vs Duty cycle

Fig. 5. Effect of input parameters on SCD of the machined zone

The EDX results of the machined zones (Fig. 6) for different tools are shown in Fig. 7. (Fig. 7(a)) shows that while using the solid copper tool, a moderate amount of copper gets transferred to the machined zone with an increased percentage of carbon and oxygen. The dissociation of the hydrocarbon type dielectric fluid during the spark process results in a larger percentage of carbon deposition on the tool material. This phenomenon leads to the formation of metal carbides and deposition on the machined surfaces with the formation of white layer. A significant amount of oxygen in the machined zone causes evaporation and melting of the work surface during the machining process (Ref 11). The presence of elements like copper and tungsten in the tool gets transferred onto the machined surfaces (Fig. 7(b)-(d)) while using MWS tools. The higher atomic radius of the element boron leads to proper bonding with the tool material which was absent from the

machined zone as confirmed by the EDX analysis. The higher deposition rate of the tool material element on the machined zone was observed with increasing reinforcement percentage in the electrode. A similar observation was made in earlier research during the surface modification process using W-Cu composite tool(Ref 10).

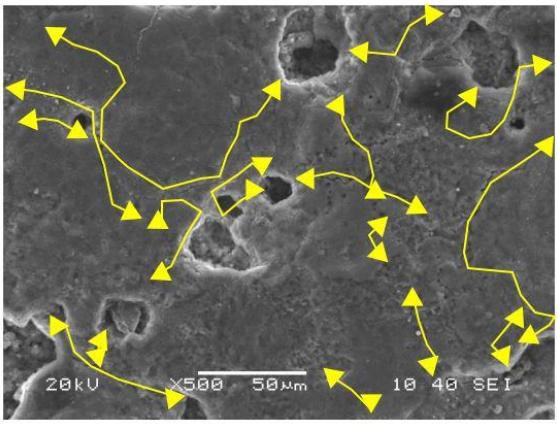

(a) SCD= 0.018596 µm/µm^{2}for solid copper tool (Ex 2)

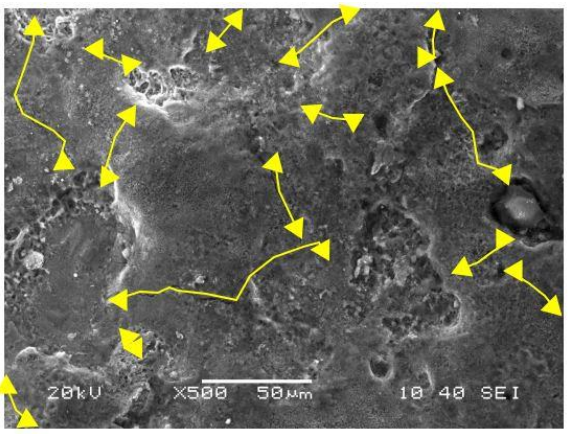

(b) SCD= 0.008491 µm/µm^2 for $Cu_{90}W_5(B_4C)_5$ MWS tool (Ex 6)

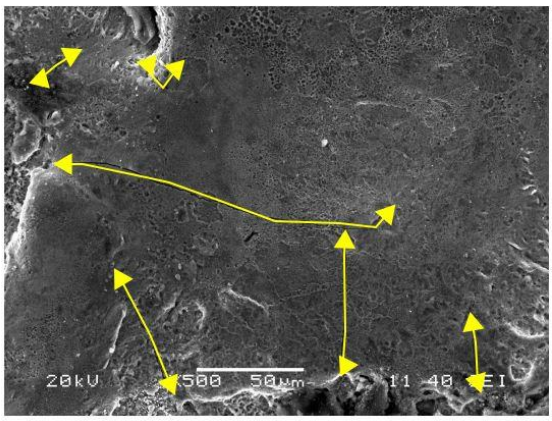

(c) SCD=0.006105µm/µm^2 for $Cu_{80}W_{10}(B_4C)_{10}$ MWS tool (Ex 10)

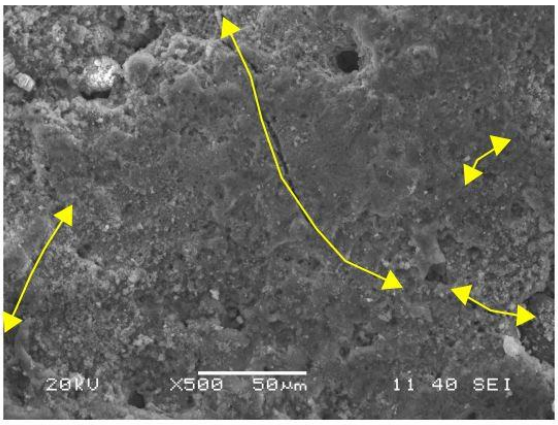

(d) SCD= 0.005965 µm/µm^2 for $Cu_{70}W_{15}(B_4C)_{15}$ MWS tool (Ex 14)

Fig. 6. SCD of different tools

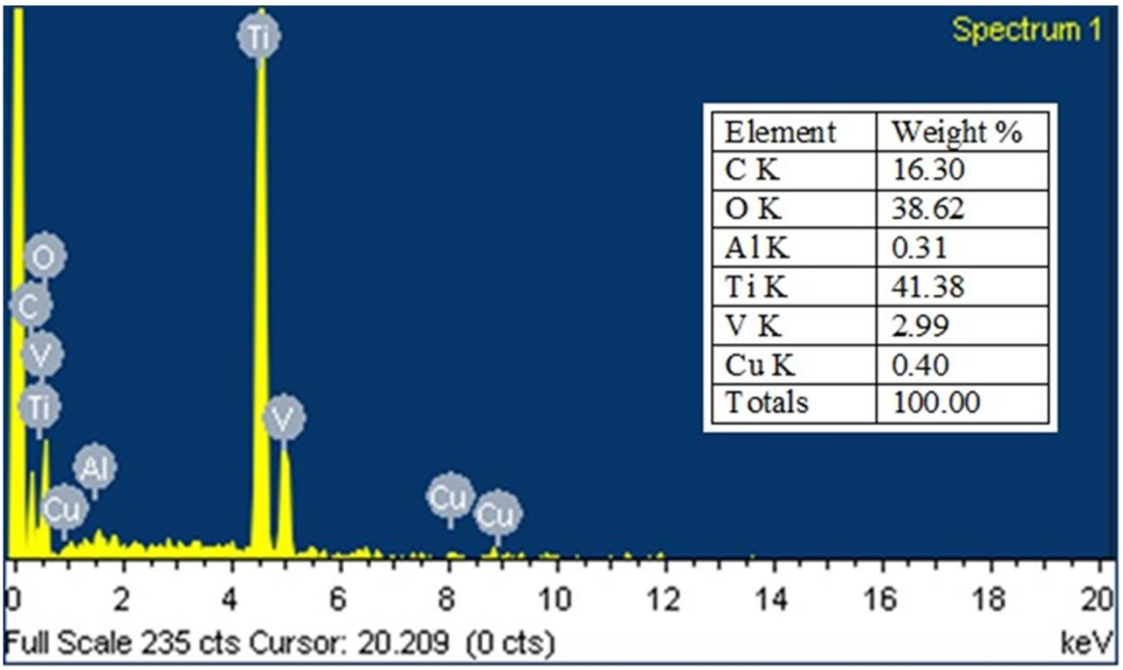

(a) Solid copper tool (Ex 2)

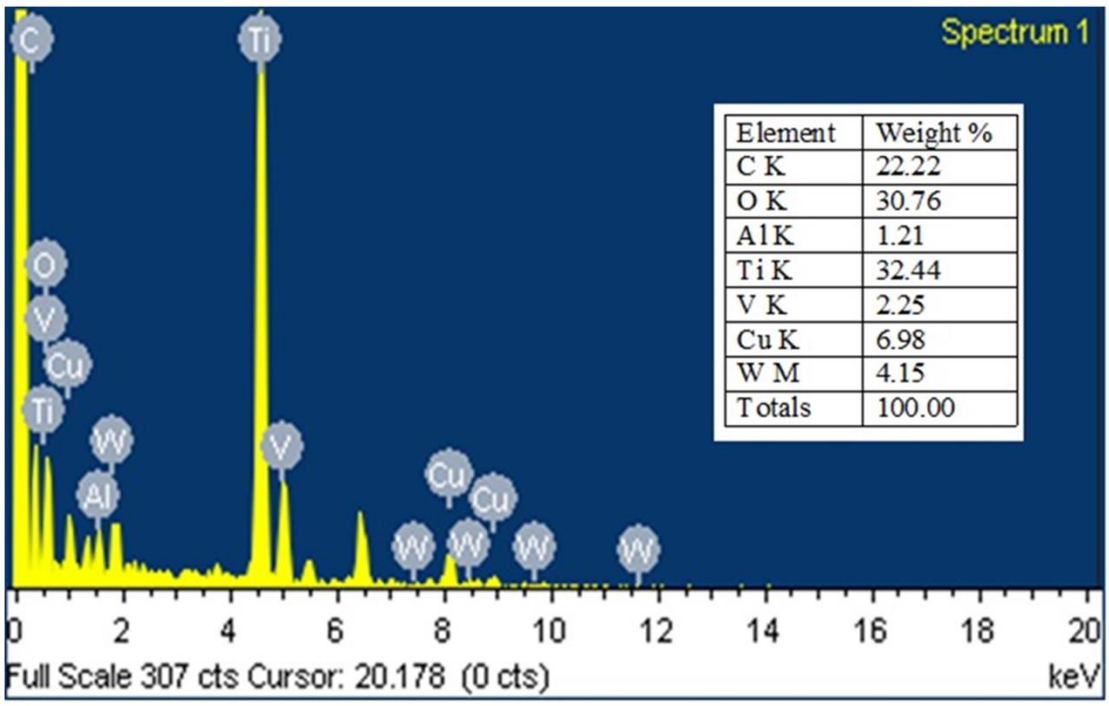

(b) $Cu_{90}W_5(B_4C)_5$ MWS tool (Ex 6)

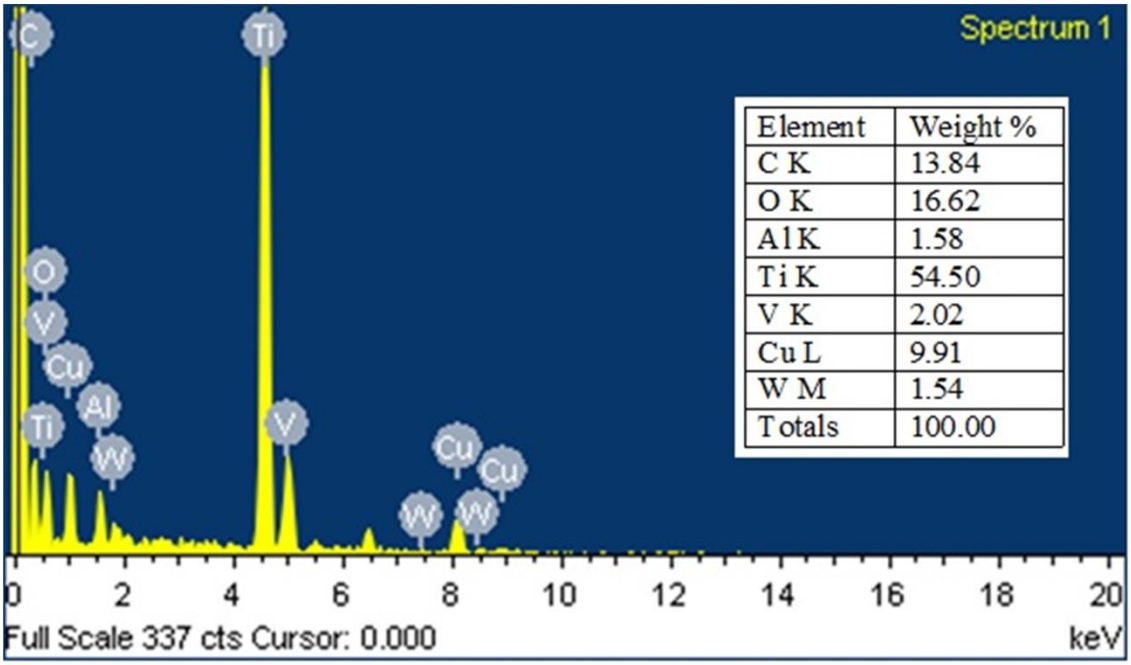

(c) $Cu_{80}W_{10}(B_4C)_{10}$ MWS tool (Ex 10)

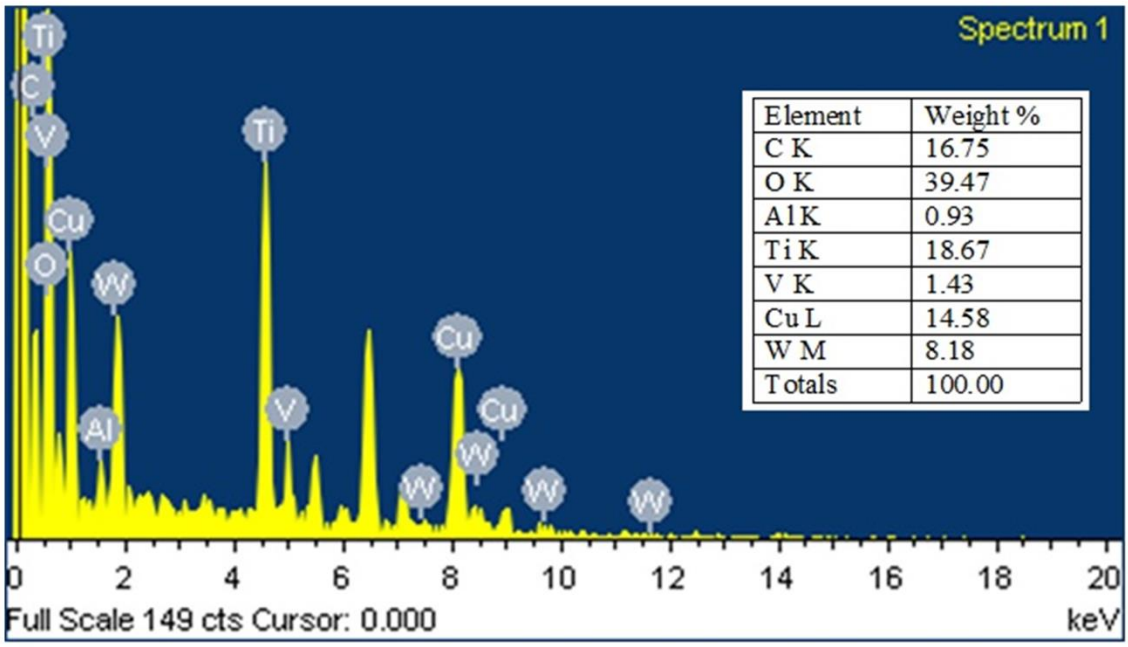

(d) $Cu_{70}W_{15}(B_4C)_{15}$ MWS tool (Ex 14)

Fig.7. EDX of machined zones while using different tools

The XRD analysis of the machined zones is presented in Fig. 8. The formation of the metal carbides and dissociation of the tool material on the work surface is prominently noticeable. Due to the formation of these metal carbides on the machined surfaces, higher resistance was observed in the machined zone. Metal carbides like VC and TiC formed over the machined zone using a solid copper tool (Fig. 8. (a)). Similarly, VC, TiC, Al_3V_7, Cu and W were seen in the machined zone while using $Cu_{90}W_5(B_4C)_5$ MWS tool. TiC and Cu presented in the machine zone were seen while using $Cu_{80}W_{10}(B_4C)_{10}$ MWS tool. VC, TiC, Cu and AlCu formed over the machined zone with the use of

$Cu_{70}W_{15}(B_4C)_{15}$ MWS tool. The formation of these composites on the machined zones in form of WLT increases the micro-hardness of the machined zones. In a similar work by Gill and Kumar (Ref 9) the formation of Fe_3C, Fe-C and Mn_7C_3 was reported to be present in the machined zone of die steel with the use of Cu-Mn tool material. These carbide phases in the machined zone have potential towards the higher surface resistance application in the industry. Uniform distribution of these phases over the machined zone was observed through the EDX spectrum (Fig. 7). From the XRD spectrum of the machined zone, it was also observed that the machining zone obtained by using a solid copper tool had fewer secondary phases compared to the composite tool material. It is further expected that the composite tool can be widely employed by the surface modification of different hard metallic alloys owing to their unique advantages such as higher micro hardness and greater wear resistance. Thus, it is anticipated that the sintered composite tool can have promising results for machining hard alloys.

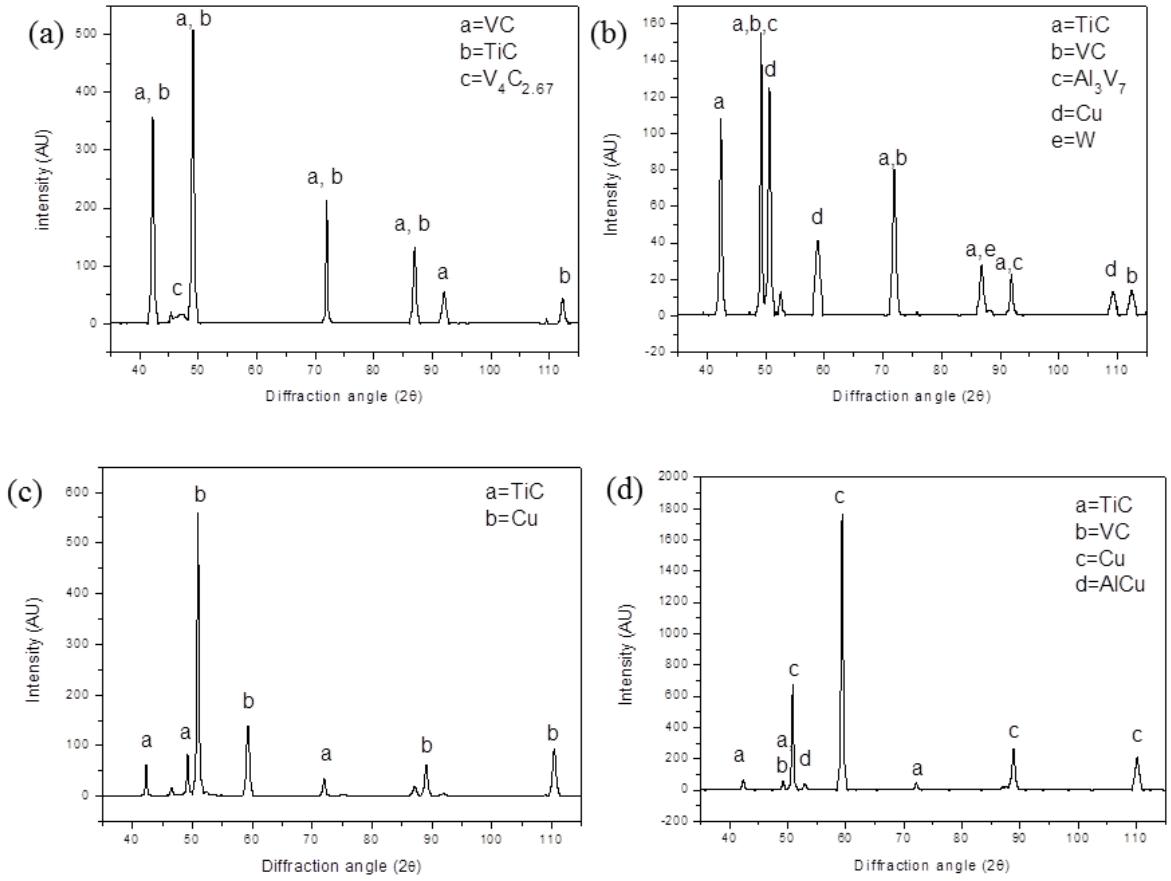

Fig. 8. XRD result of the machined surfaces by different tools (a) Solid copper tool (Ex 2), (b) $Cu_{90}W_5(B_4C)_5$ MWS tool (Ex 6), (c) $Cu_{80}W_{10}(B_4C)_{10}$ MWS tool (Ex 10) and (d) $Cu_{70}W_{15}(B_4C)_{15}$ MWS tool (Ex 14)

3.5. Effect of input parameters on WLT

The effect of parameters on WLT is shown in Fig. 9. Similarly, the box-plot for WLT is shown in Supplementary Fig. 5 to show the variation of WLT at different parametric conditions. The WLT

for $Cu_{90}W_5(B_4C)_5$ MWS tool showed a lower value compared to other tools. However, a higher percentage of reinforcement showeda significant effect on the WLT. The micro-graphs of WLT using different tools are shown in Fig. 10. The WLT rises with an increase in peak current and duty factor due to facts related to the higher TWR as discussed in the previous section for MWS tool material. However, initial increase and decreasing trends of WLT were observed with higher pulse-on-time due to non-uniform deposition of material on the machined zone. The WLT consists of metallic carbides like TiC, VC, B_4C, and WC that increases the micro-hardness of the WLT as observed from the EDX of the surface. The box plot shown in Supplementary Fig. 5 confirms that the variation in WLT is reasonably higher with the use of $Cu_{70}W_{15}(B_4C)_{15}$ tool.

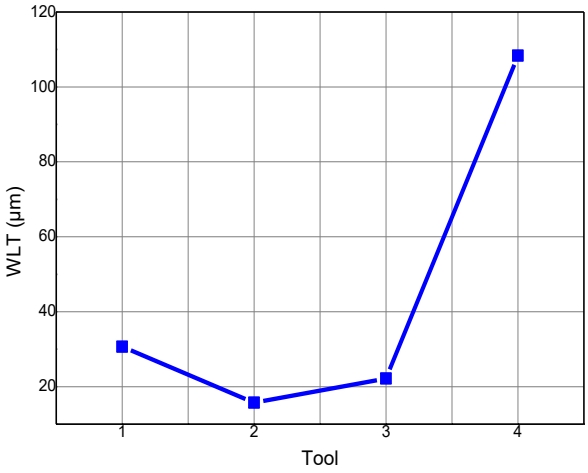

(a) WLT vs Tool type

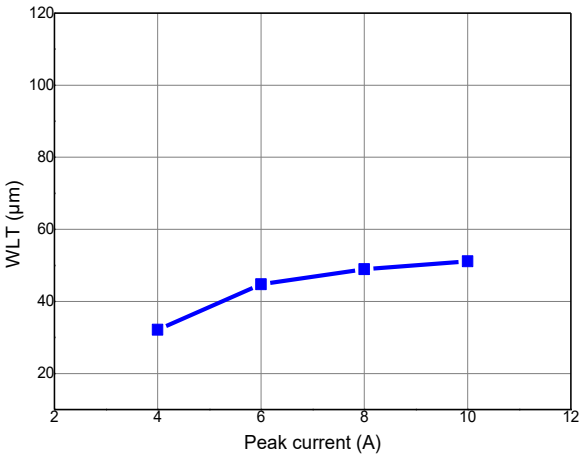

(b) WLT vs Peak current

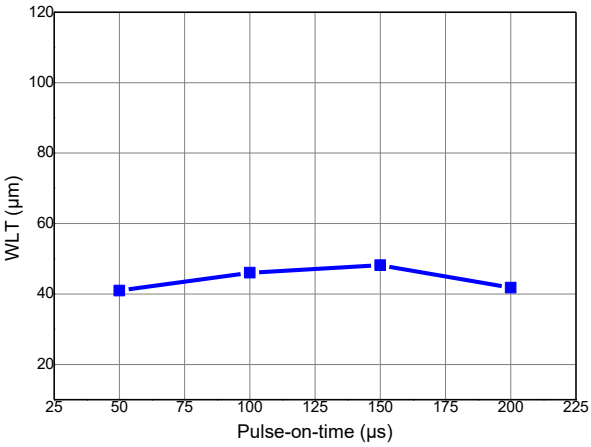

(c) WLT vs Pulse-on-time

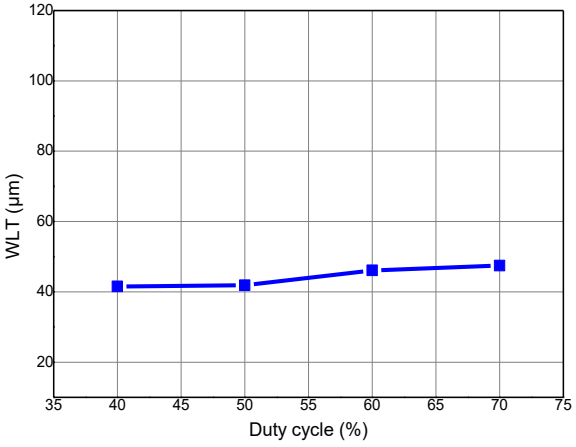

(d) WLT vs Duty cycle

Fig. 9. Effect of parameters on WLT

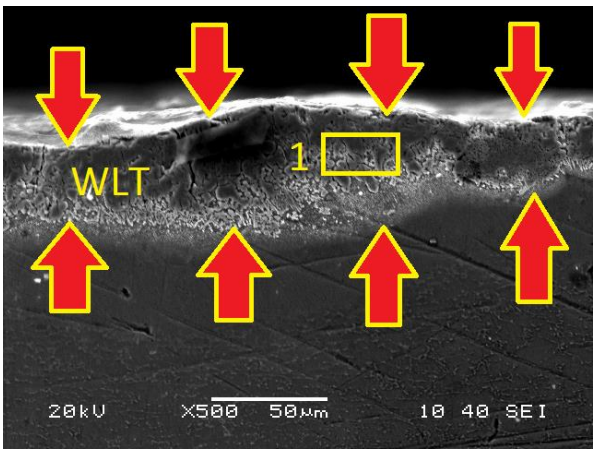

(a) WLT= 33.067 µm for solid copper tool at 500× (Ex 2)

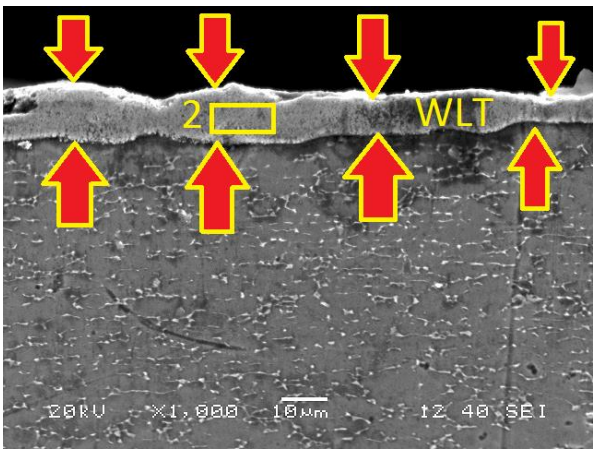

(b) WLT= 8.436 µm for $Cu_{90}W_5(B_4C)_5$ MWS tool at 1000× (Ex 6)

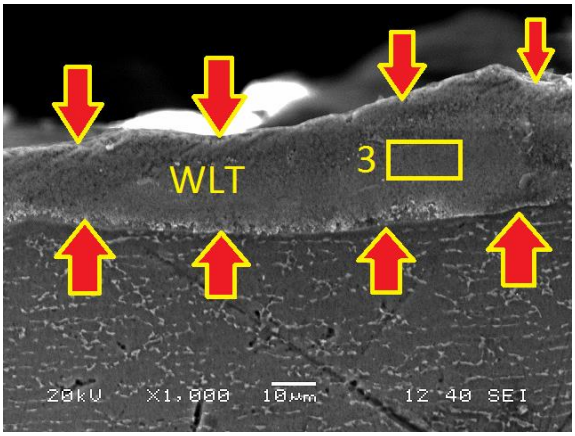

(c) WLT= 23.894 µm for $Cu_{80}W_{10}(B_4C)_{10}$ MWS tool at 1000× (Ex 10)

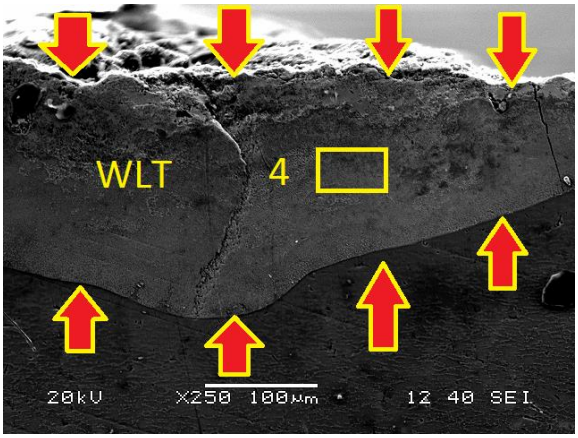

(d) WLT= 113.597 µm for $Cu_{70}W_{15}(B_4C)_{15}$ MWS tool at 250× (Ex 14)

Fig. 10. WLT for different tools

The EDX of the WLT marked as region 1-4 in Fig. 10 is shown in Fig. 11. Here, copper was seen present on the WLT formed by using a solid copper tool (Fig. 11 (a)) with an increased percentage of carbon. Likewise, tool elements copper and tungsten present on the WLT formed by the use of MWS tools is shown in Fig. 11 (b)-(d). Here, likewise increased percentages of carbon and oxygen were present in the WLT while using MWS tools.

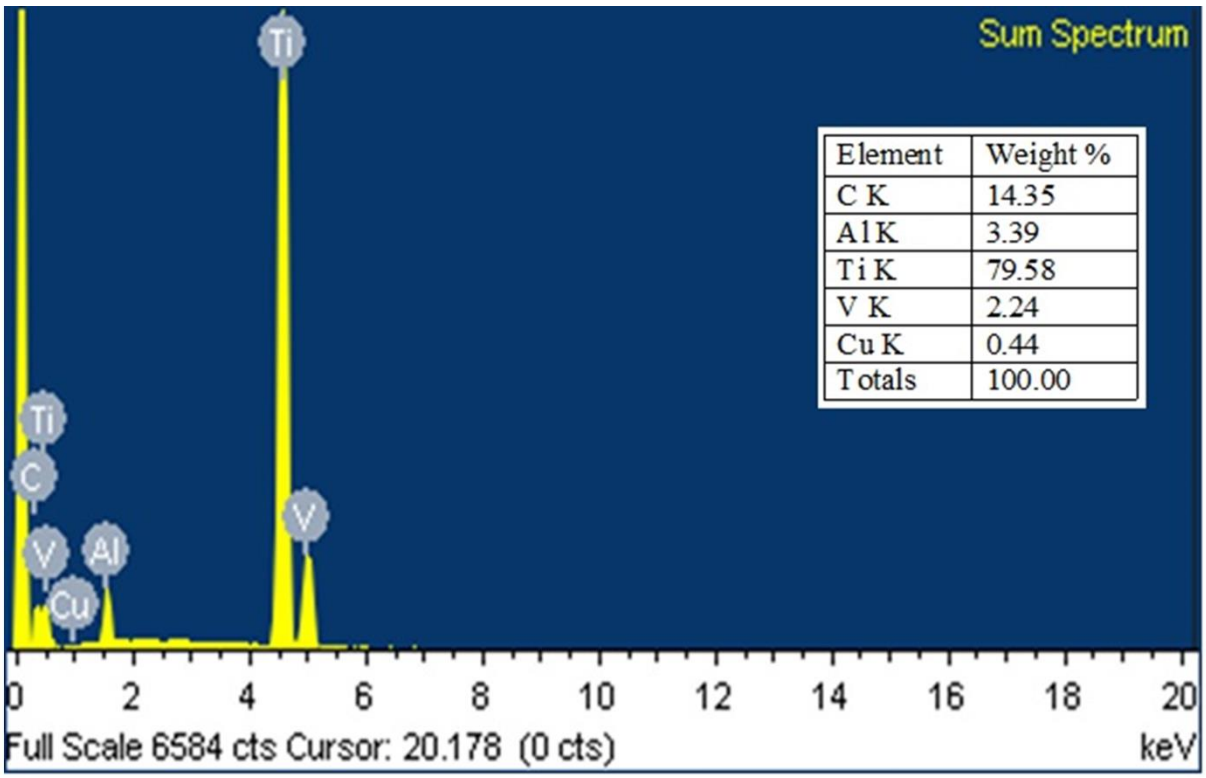

Element	Weight %
C K	14.35
Al K	3.39
Ti K	79.58
V K	2.24
Cu K	0.44
Totals	100.00

(a) Solid copper tool (Ex 2)

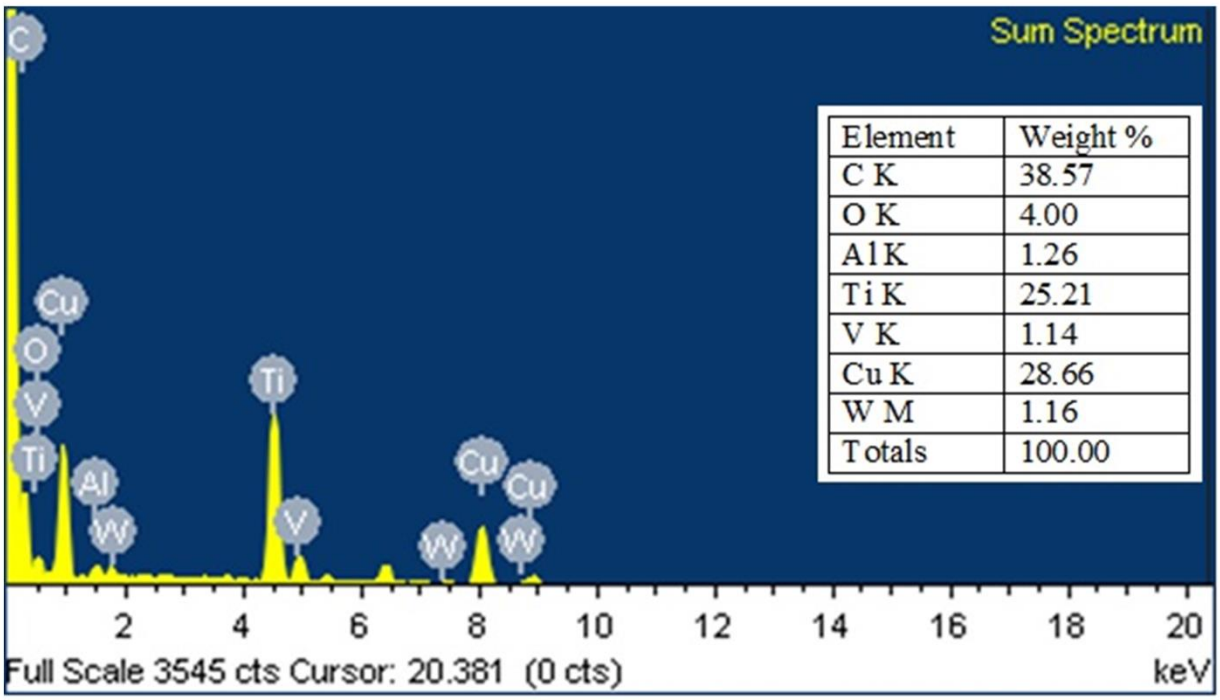

Element	Weight %
C K	38.57
O K	4.00
Al K	1.26
Ti K	25.21
V K	1.14
Cu K	28.66
W M	1.16
Totals	100.00

(b) $Cu_{90}W_5(B_4C)_5$ MWS tool (Ex 6)

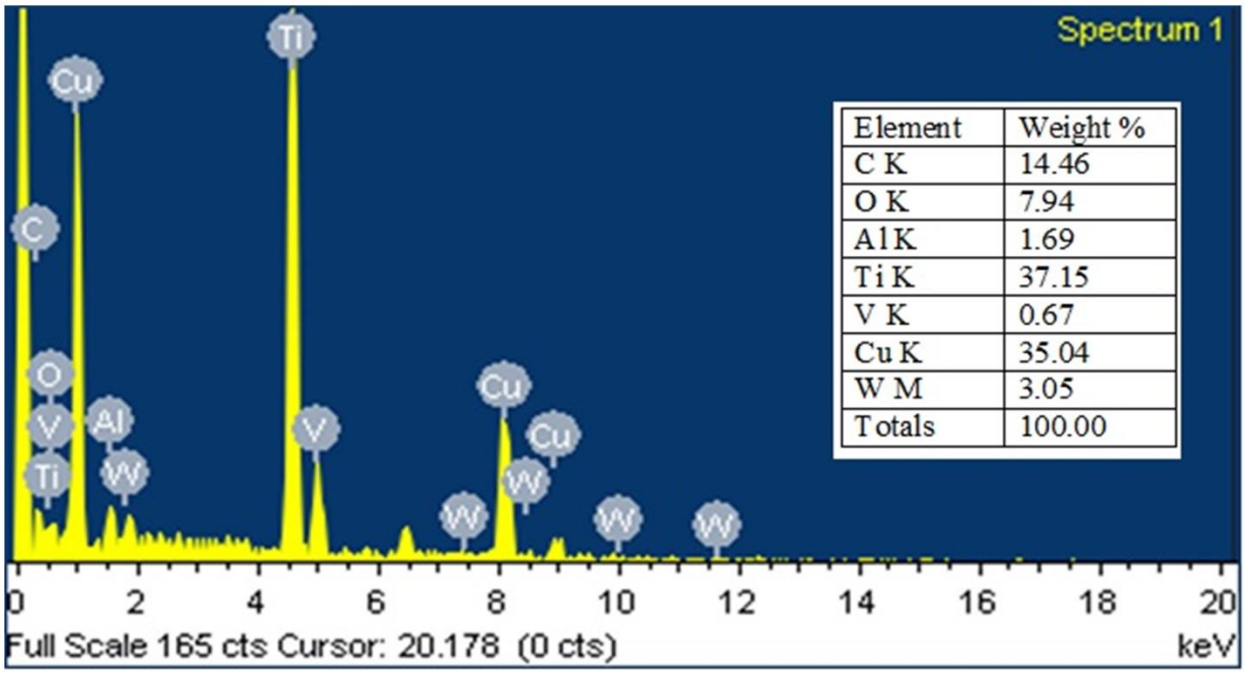

(c) $Cu_{80}W_{10}(B_4C)_{10}$ MWS tool (Ex 10)

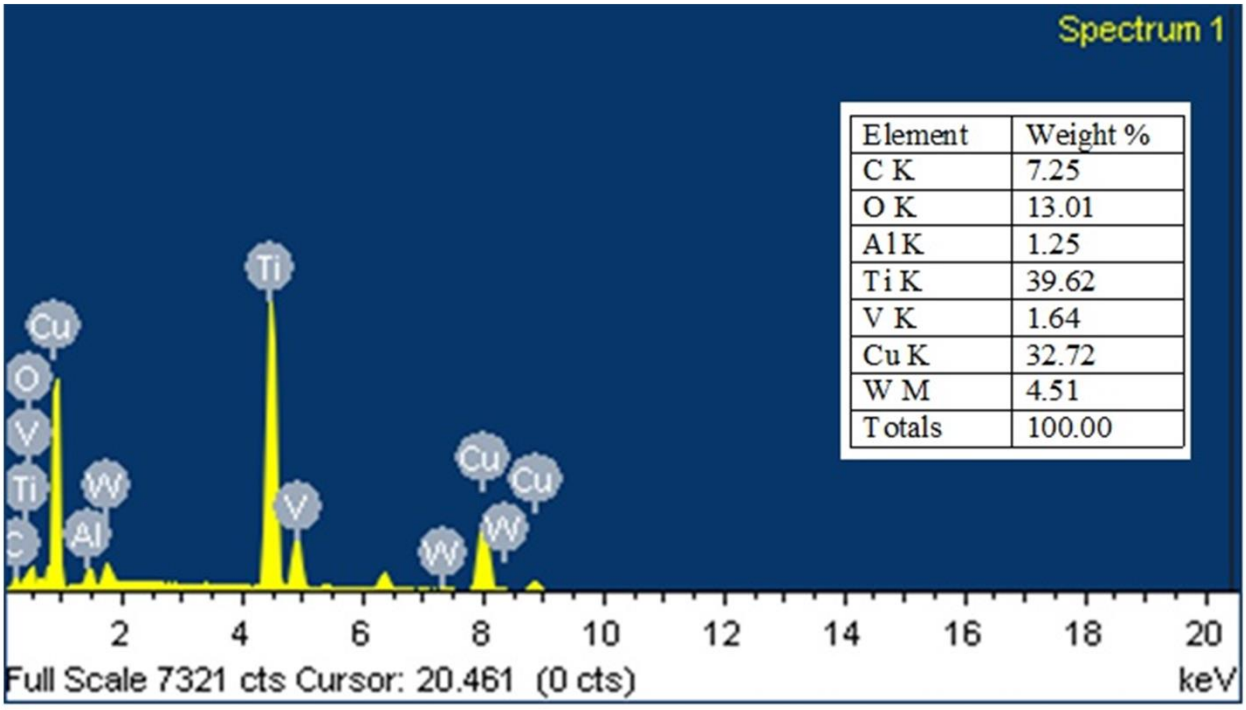

(d) Cu70W15(B4C)15 MWS tool (Ex 14)

Fig. 11. EDX on the WLT for different tools

3.6. Effect of input parameters on MH

The effect of input parameters on the MH of the WL is shown in Fig. 12. Similarly, the box-plot for MH is shown in Supplementary Fig. 6 to show the variation of MH under different parametric conditions. The lowest MH was observed with the use of a solid copper tool. The harder carbide and metallic phase (W and B_4C) on the composite tool material leads to the increase in the MH value of the machined zone. The MH on the WL increases due to the formation of metal carbides like TiC,

VC, B_4C, and WC and the formation of different metal carbides was confirmed by the phase transformation on the machined surface from the XRD analysis. The increasing trends of MH value were noticed for higher peak current and pulse on time for the MWS material. The box plot shown in Supplementary Fig. 6 confirmed that the variation in MH was reasonably higher with the use of $Cu_{70}W_{15}(B_4C)_{15}$ tool.

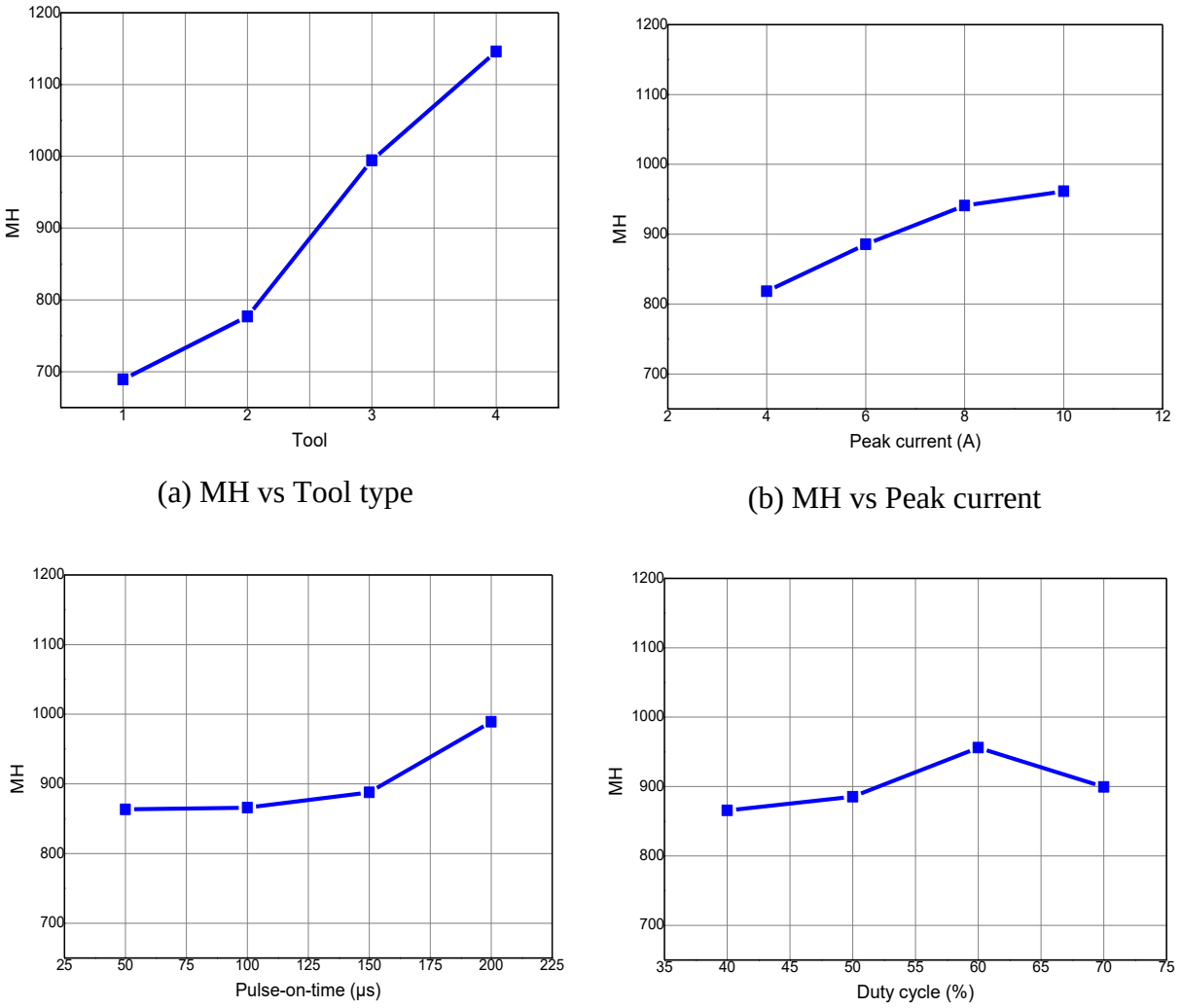

(a) MH vs Tool type

(b) MH vs Peak current

(c) MH vs Pulse-on-time

(d) MH vs Duty cycle

Fig. 12. Effect of parameters on MH

3.7 ANOVA to evaluate machining performance

A statistical analysis tool, analysis of variance (ANOVA) was performed in the software Minitab 17 to evaluate the machining performance in all cases. The ANOVA results are presented in Table 3. The coefficient of determination (R^2) value for MRR, TWR, R_a, SCD, WLT and MH were found to be 95.5%, 95.0%, 98.6%, 99.9%, 98.6% and 96.5% respectively. From ANOVA (Table 3), it was found that the tool materials can be very significant in influencing the machining outcome

From the factorial plots, the optimal conditions were obtained as $A_1B_1C_4D_4$, $A_1B_1C_4D_1$, $A_1B_1C_1D_2$, $A_4B_1C_1D_3$, $A_2B_1C_1D_1$ and $A_1B_1C_1D_1$ for MRR, TWR, R_a, SCD, WLT and MH respectively.

Table 3. ANOVA of machining performances

Parameters	DF	MRR		TWR		R_a		SCD		WLT		MH	
		SS	P	SS	P	SS	P	SS	P	SS	P	SS	P
A:Tool type	3	8.1157	0.020*	52.685	0.024*	154.404	0.003*	0.000542	0.000*	22393.9	0.003*	515158	0.015*
B:Peak current	3	0.4306	0.512	3.655	0.471	4.221	0.314	0.000034	0.000*	862.4	0.222	49398	0.270
C:Pulse-on-time	3	0.6751	0.371	3.512	0.484	1.340	0.665	0.000015	0.001*	142.8	0.741	42534	0.310
D:Duty cycle	3	1.3396	0.195	3.314	0.502	2.193	0.514	0.000004	0.009*	108.5	0.804	18077	0.572
Error	3	0.4465		3.338		2.289		0.000000		324.2		22732	
Total	15	11.0075		66.504		164.446		0.000595		23831.8		647900	

*Significant parameters at level of significance of 5%

4. Conclusion

In this study, a newly fabricated microwave sintered composite (MWS) composite tool fabricated from different types of materials in various compositions of copper, tungsten and boron carbide were used for electro-discharge machining ofTi6Al4V. The results obtained through this experiment provided an important direction for the use of composite tools prepared by the MWS process. It was found that an increase in the weight percentage of the reinforcements (W and B_4C) in the tool reduces the material removal rate as well as increases the tool wear during EDM. Similarly, an increase in the percentage of *W* and B_4C in the MWS tool worsen the surface roughness. However, increasing the content of the reinforcement of *W* and B_4C in the copper matrix reduces the surface crack density of the machined zone with the MWS tool. The $Cu_{90}W_5(B_4C)_5$ tool showed a lower extent of white layer in comparison to the other MWS tools. Strong interfacial bonding between the matrix and reinforcement results in lowering the erosion of the tool surface. From the current work, it can be interpreted that the MWS tool of $Cu_{90}W_5(B_4C)_5$ is suitable to machine hard alloys (i.e. Ti6Al4V) as it generated a lower amount of debris in the machined zone. As far as MRR, TWR and R_a are considered, solid copper tool performed better as compared to the MWS tools. However, the $Cu_{70}W_{15}(B_4C)_{15}$ MWS tool was found suitable for surface coating of a hard composite layer on the work piece surface rather than machining. The EDX analysis of the machined surfaces revealed the transfer of copper and tungsten onto the machined surfaces. The debris of work piece material and

tool material gets deposited on the machined surface to form the white layer which consists of metal carbides like TiC and VC. The formation of metal carbides in the machining areas increases the micro-hardness of the white layer.

Conflict of interest: The authors declare no conflict of interest.

Acknowledgements:

All authors greatly acknowledge the financial support provided by the UKRI via Grants No. EP/L016567/1, EP/S013652/1, EP/S036180/1, EP/T001100/1 and EP/T024607/1, TFIN+ Feasibility study award to LSBU (EP/V026402/1), the Royal Academy of Engineering via Grants No. IAPP18-19\295 and TSP1332, EURAMET EMPIR A185 (2018), the EU Cost Action (CA15102, CA18125, CA18224 and CA16235) and the Newton Fellowship award from the Royal Society (NIF\R1\191571). Wherever applicable, the work made use of Isambard Bristol, UK supercomputing service accessed by a Resource Allocation Panel (RAP) grant as well as ARCHER resources (Project e648).

References

[1] P.K. Patowari, P. Saha, and P.K. Mishra, An experimental investigation of surface modification of C-40 steel using W–Cu powder metallurgy sintered compact tools in EDM. The International Journal of Advanced Manufacturing Technology 2015; 80(1–4):343–60.

[2] P.K. Patowari, P. Saha, and P.K. Mishra, Artificial neural network model in surface modification by EDM using tungsten-copper powder metallurgy sintered electrodes. The International Journal of Advanced Manufacturing Technology 2010; 51(5–8):627-38.

[3] P.K. Patowari, P. Saha, and P.K. Mishra, Taguchi analysis of surface modification technique using W-Cu powder metallurgy sintered tools in EDM and characterization of the deposited layer. The International Journal of Advanced Manufacturing Technology 2011; 54(5-8):593-604.

[4] M.E. Krishna, and P.K. Patowari, Parametric study of electric discharge coating using powder metallurgical green compact electrodes. Materials and Manufacturing Processes 2014; 29(9):1131-8.

[5] T.A. El-Taweel, Multi-response optimization of EDM with Al-Cu-Si-TiC P/M composite electrode. The International Journal of Advanced Manufacturing Technology 2009; 44(1-2):100-13.

[6] A.K. Khanra, B.R. Sarkar, B. Bhattacharya, L.C. Pathak, and M.M. Godkhindi, Performance of ZrB2-Cu composite as an EDM electrode. Journal of Materials Processing Technology 2007; 183(1):122-6.

[7] P. Balasubramanian, and T. Senthilvelan, A Comparative study on the Performance of Different Sintered Electrodes in Electrical Discharge Machining. Transaction of Indian Institute of Metals 2014; 68(1):51-9.

[8] C. Cogun, Z. Esen, A. Genc, F. Cogun, and N. Akturk, Effect of powder metallurgy Cu-B4C electrodes on workpiece surface characteristics and machining performance of electric discharge machining. Proceedings of the Institution of Mechanical Engineers, Part B: Journal of Engineering Manufacture 2016; 230(12):2190-203.

[9] A.S. Gill, and S. Kumar, Surface Roughness and Microhardness Evaluation for EDM with Cu-Mn Powder Metallurgy Tool. Materials and Manufacturing Processes 2016; 31(4):514-21.

[10] M. Rahang, and P.K. Patowari, Parametric Optimization for Selective Surface Modification in EDM Using Taguchi Analysis. Materials and Manufacturing Processes 2016; 31(4):422-31.

[11] B. Singh, J. Kumar, and S. Kumar, Optimization and surface modification in electrical discharge machining of AA 6061/SiCp composite using Cu-W electrode. Proceedings of the Institution of Mechanical Engineers, Part L: Journal of Materials: Design and Applications 2017; 231(3):332-48.

[12] P. Goyal, N.M. Suri, S. Kumar, and R. Kumar, Investigating the surface properties of EN-31 die-steel after machining with powder metallurgy EDM electrodes. Materials Today: Proceedings 2017; 4(2):3694-700.

[13] P.J. Liew, Z. Nurlishafiqa, Q. Ahsan, T. Zhou, and J. Yan, Experimental investigation of RB-SiC using Cu–CNF composite electrodes in electrical discharge machining. The International Journal of Advanced Manufacturing Technology 2018; 98(9–12):3019-28.

[14] P.M. Kumar, K. Sivakumar, and N. Jayakumar, Multiobjective optimization and analysis of copper–titanium diboride electrode in EDM of monel 400^{TM} alloy. Materials and Manufacturing Processes 2018; 33(13):1429-37.

[15] P.K. Patowari, U.K. Mishra, P. Saha, and P.K. Mishra, Surface Integrity of C-40 Steel Processed with WC-Cu Powder Metallurgy Green Compact Tools in EDM. Materials and Manufacturing Processes 2011; 26:668-676.

[16] M.S. Shunmugam, P.K. Philip, and A. Gangadhar, Improvement of wear resistance by EDM with tungsten carbide P/M electrode. Wear 1994; 171:1-5.

[17] A. Gangadhar, M.S. Shunmugam, and P.K. Philip, Surface modification in electro discharge processing with a powder compact tool electrode. Wear 1991; 143(1):45-55.

[18] M.P. Samuel, and P.K. Philip, Power metallurgy tool electrodes for electrical discharge machining. International Journal of Machine Tools and Manufacture 1997; 37(11):1625-33.

[19] J.D. Marafona, Black layer affects the thermal conductivity of the surface of copper-tungsten electrode. The International Journal of Advanced Manufacturing Technology 2009; 42(5–6):482-8.

[20] J. Marafona, and C. Wykes, New method of optimising material removal rate using EDM with copper-tungsten electrodes. International Journal of Machine Tools and Manufacture 2000; 40(2):153-64.

[21] K.M. Shu, and G.C. Tu, Fabrication and characterization of Cu-SiCp composites for electrical discharge machining applications. Materials and Manufacturing Processes 2001; 16(4):483-502.

[22] L. Li, Y.S. Wong, J.Y.H. Fuh, and L. Lu, Effect of TiC in copper-tungsten electrodes on EDM performance. Journal of Materials Processing Technology 2001; 113(1–3):563-7.

[23] L. Li, Y.S. Wong, J.Y.H. Fuh, and L. Lu, EDM performance of TiC/copper-based sintered electrodes. Materials abd Design 2001; 22(8):669-78.

[24] L. Li, Z.W. Niu, and G.M. Zheng, Ultrasonic Electro deposition of Cu-SiC Electrodes for EDM. Materials and Manufacturing Processes 2016; 31(1):37-41.

[25] N.K. Bhoi, H. Singh, S. Pratap, and P.K. Jain, Microwave material processing : a clean, green, and sustainable approach. Sustainable Engineering Products and Manufacturing Technologies. 1st ed., In: K. Kumar, D. Zindani and P. Davim Ed., Academic Press Elsevier, 2019, p 3-23.

[26] N.K. Bhoi, H. Singh, and S. Pratap, Developments in the aluminum metal matrix composites reinforced by micro/nano particles–A review. Journal of Composite Materials 2020; 54(6):813-33.

[27] N.K. Bhoi, H. Singh, and S. Pratap, Synthesis and characterization of zinc oxide reinforced aluminum metal matrix composite produced by microwave sintering. Journal of Composite Materials 2020; doi: 10.1177/0021998320918646.

[28] C. Maniere, S. Chan, and E.A. Olevsky, Microwave sintering of complex shapes: from multiphysics simulation to improvements of process scalability. Journal of American Ceramic Society 2019; 102:611- 620.

[29] A.K. Sahu, and S.S. Mahapatra, Performance analysis of tool electrode prepared through laser sintering process during electrical discharge machining of titanium. The International Journal of Advanced Manufacturing Technology 2020; 106:1017-1041.

[30] A.K. Sahu, and S.S. Mahapatra, Surface Characteristics of EDMed Titanium Alloy and AISI 1040 Steel Workpieces Using Rapid Tool Electrode. Arabian Journal for Science and Engineering 2020; 45:699-718.

Supplementary materials

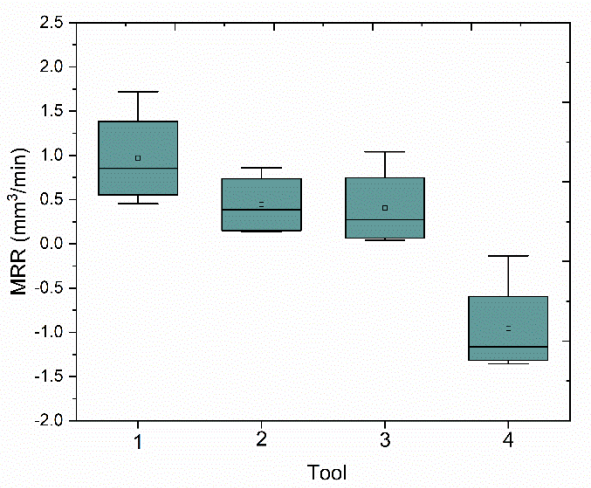

(a) MRR vs Tool type

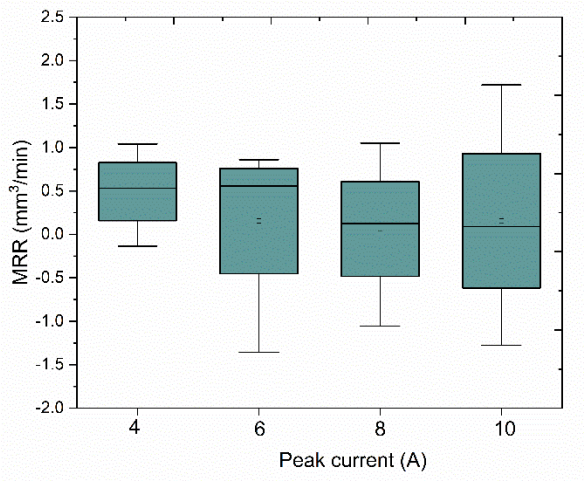

(b) MRR vs Peak current

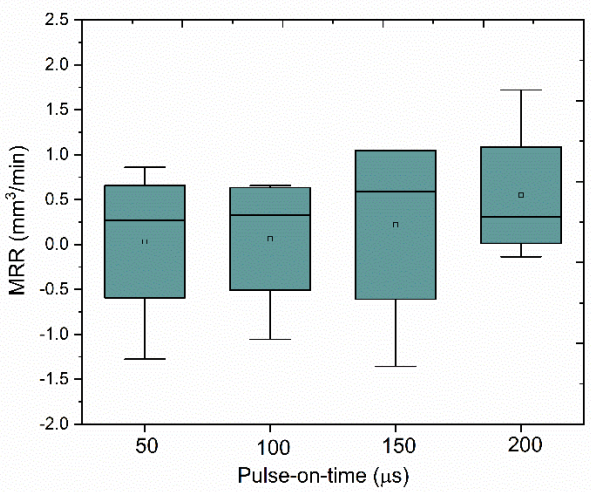

(c) MRR vs Pulse-on-time

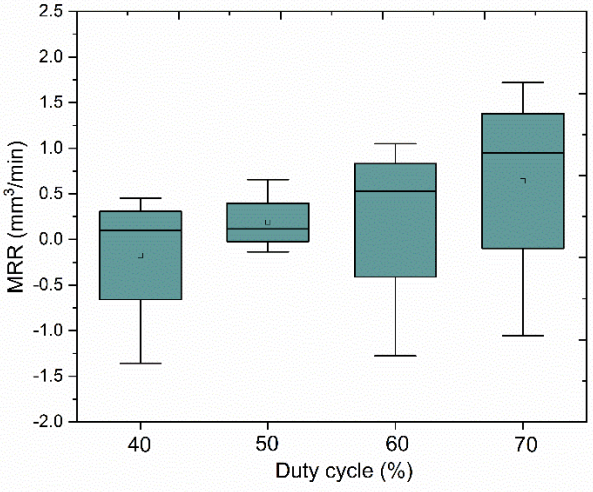

(d) MRR vs Duty cycle

Supplementary Fig. 1. Effect of input parameters on MRR

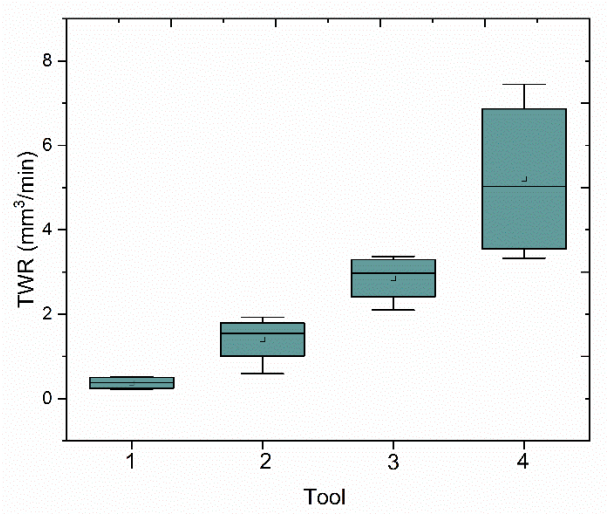

(a) TWR vs Tool type

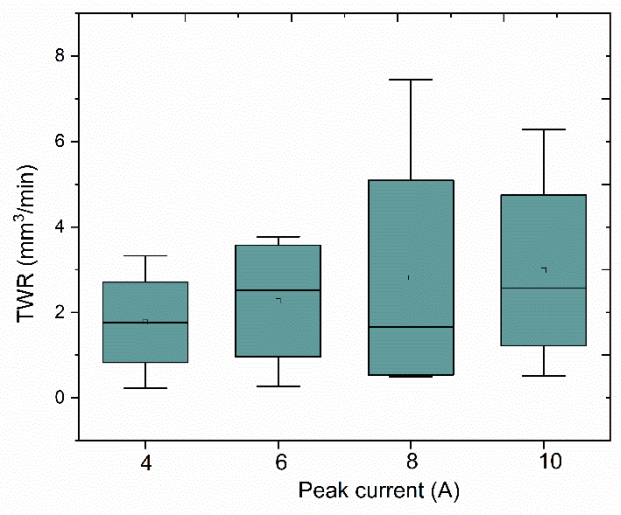

(b) TWR vs Peak current

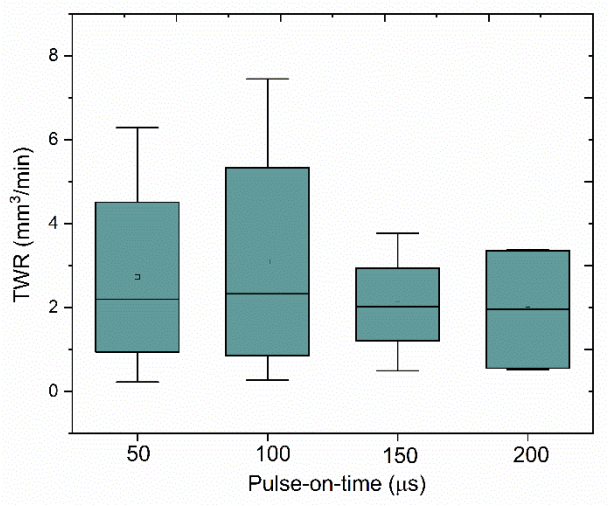

(c) TWR vs Pulse-on-time

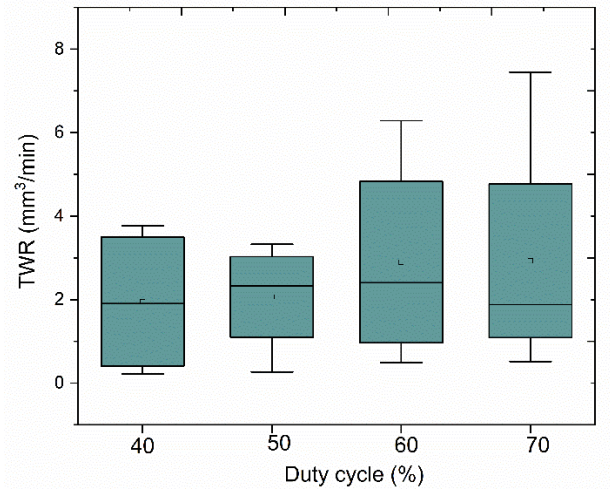

(d) TWR vs Duty cycle

Supplementary Fig. 2. Effect of input process parameters on TWR

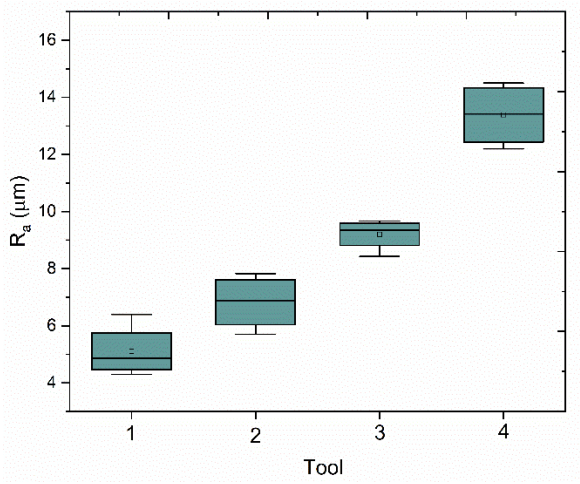

(a) R_a vs Tool type

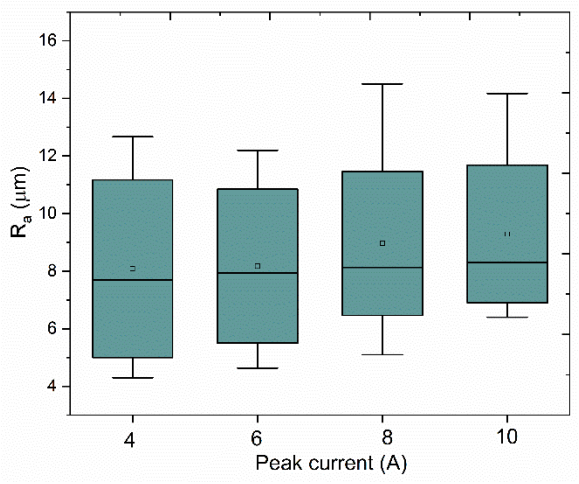

(b) R_a vs Peak current

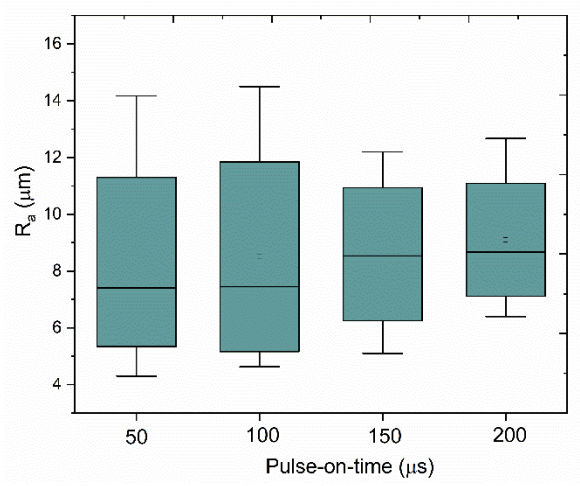

(c) R_a vs Pulse-on-time

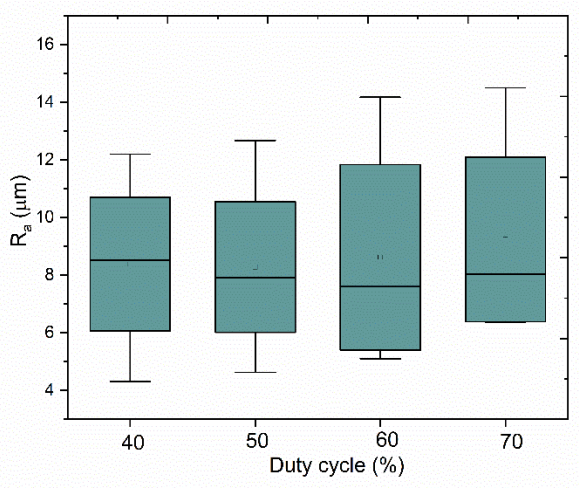

(d) R_a vs Duty cycle

Supplementary Fig. 3. Effect of input process parameters on R_a

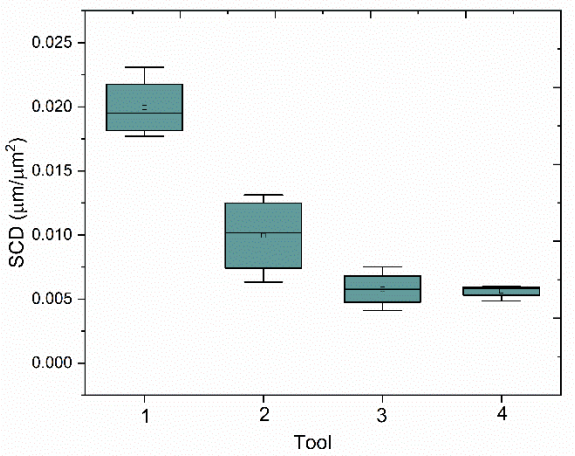

(a) SCD vs Tool type

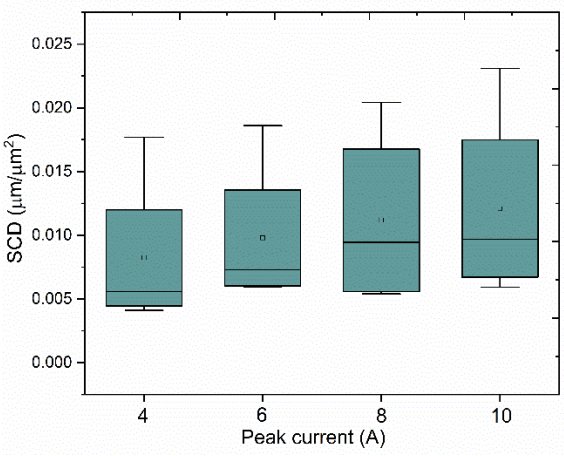

(b) SCD vs Peak current

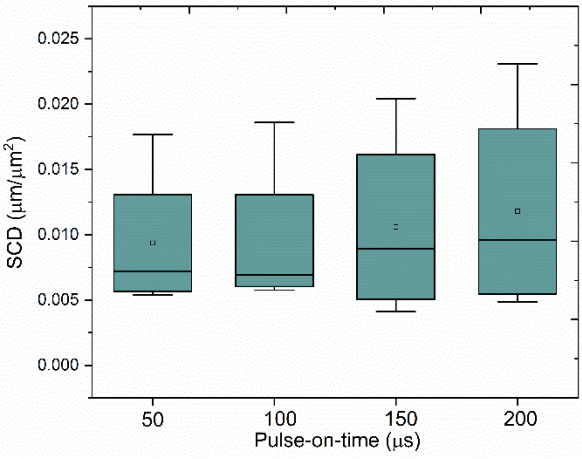

(c) SCD vs Pulse-on-time

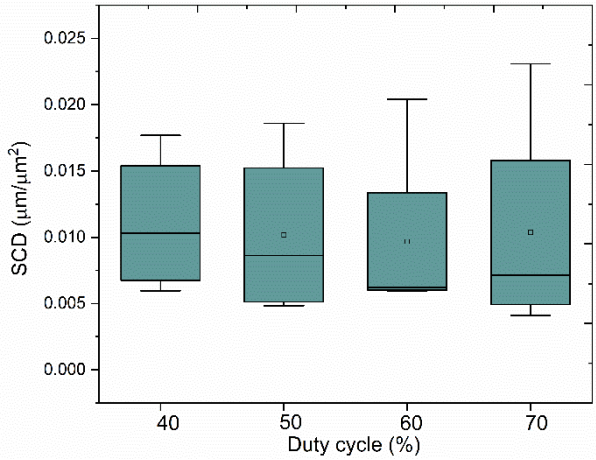

(d) SCD vs Duty cycle

Supplementary Fig. 4. Effect of input parameters on SCD of the machined zone

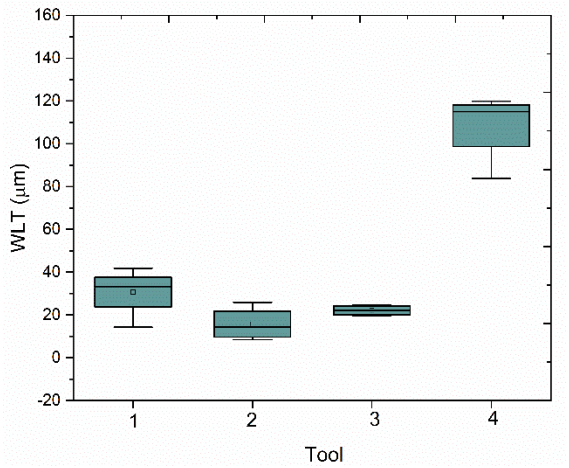

(a) WLT vs Tool type

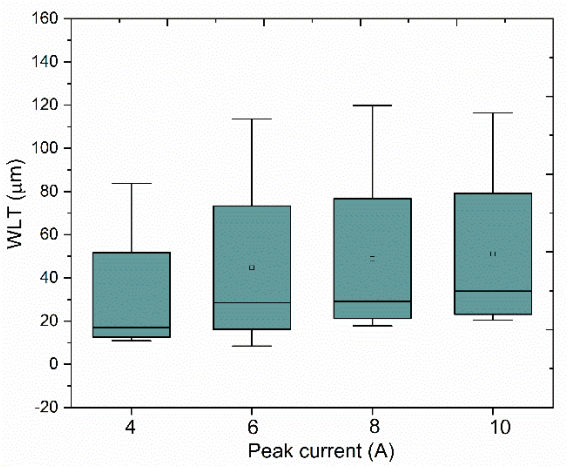

(b) WLT vs Peak current

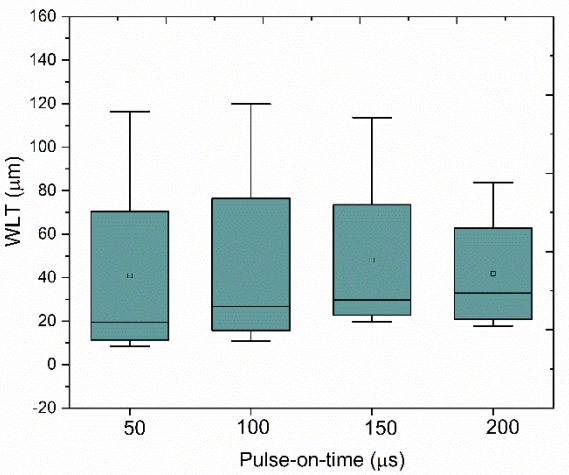

(c) WLT vs Pulse-on-time

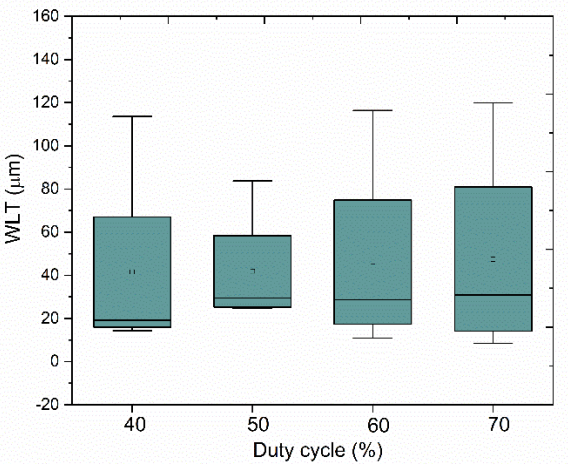

(d) WLT vs Duty cycle

Supplementary Fig. 5. Effect of parameters on WLT

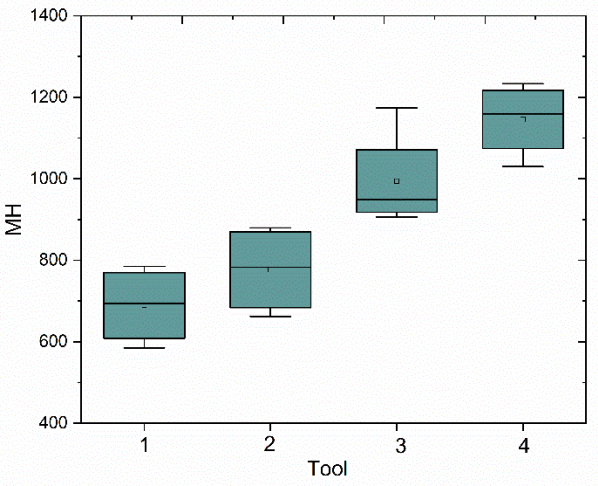

(a) MH vs Tool type

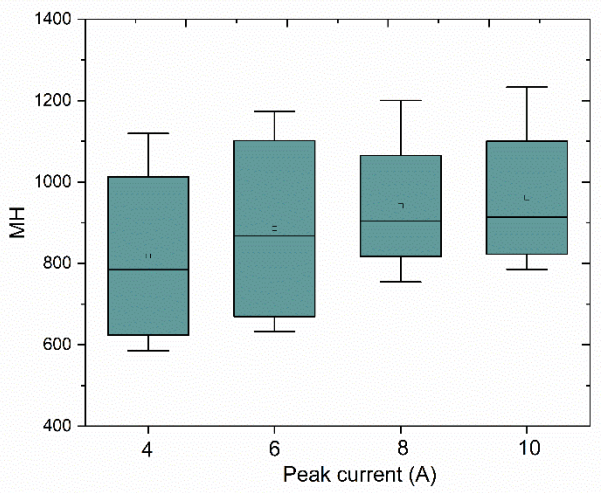

(b) MH vs Peak current

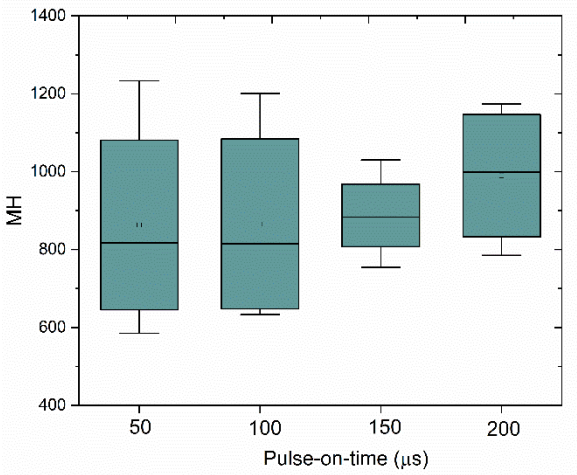

(c) MH vs Pulse-on-time

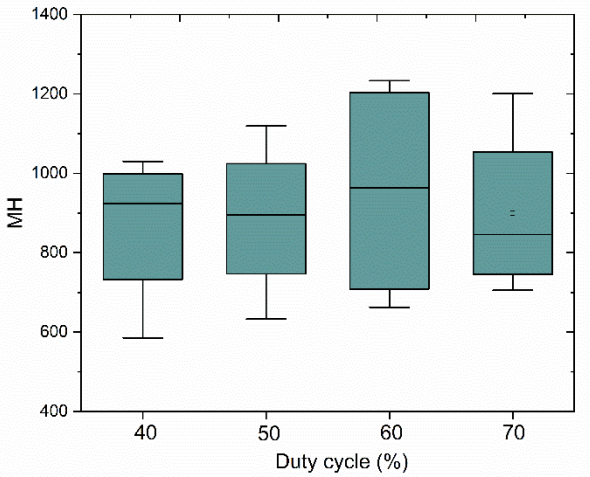

(d) MH vs Duty cycle

Supplementary Fig. 6. Effect of parameters on MH